SYNTHESIS OF POLY(DIALLYLDIMETHYLAMMONIUM CHLORIDE) COATED IRON OXIDE FOR THE DEGRADATION OF E. COLI VIA FENTON-LIKE DEGRADATION

ONG SIN HUI

A project report submitted in partial fulfilment of the requirements for the award of Bachelor of Chemical Engineering with Honours

Lee Kong Chian Faculty of Engineering and Science
Universiti Tunku Abdul Rahman

May 2023

DECLARATION

I hereby declare that this project report is based on my original work except for citations and quotations which have been duly acknowledged. I also declare that it has not been previously and concurrently submitted for any other degree or award at UTAR or other institutions.

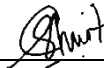Signature   :   *Sin Hui*

Name   :   Ong Sin Hui

ID No.   :   1803926

Date   :   28.04.2023

<div align="center">**APPROVAL FOR SUBMISSION**</div>

I certify that this project report entitled **"SYNTHESIS OF POLY(DIALLYLDIMETHYLAMMONIUM CHLORIDE) COATED IRON OXIDE FOR THE DEGRADATION OF E. COLI VIA FENTON-LIKE DEGRADATION"** was prepared by **ONG SIN HUI** has met the required standard for submission in partial fulfilment of the requirements for the award of Bachelor of Chemical Engineering with Honours at Universiti Tunku Abdul Rahman.

Approved by,

Signature   :

Supervisor   :   Ts. Dr. Shuit Siew Hoong

Date   :   28.04.2023

ACKNOWLEDGEMENTS

I would like to thank everyone who had contributed to the successful completion of this project. I would like to express my gratitude to my research supervisor, Ts. Dr. Shuit Siew Hoong for his invaluable advice, guidance and enormous patience throughout the development of research.

In addition, I would also like to express my gratitude to my loving parents and friends who had helped and given me encouragement throughout the period in completing my final year project.

Lastly, I offer my best regards to all who had supported me towards the completion of the final year project.

ABSTRACT

Waterborne infections are responsible for millions of deaths annually, highlighting the crucial need for effective water treatment processes to ensure public health. Consumption of contaminated water can cause severe microbial infections, leading to significant health concerns such as damage to the intestinal lining and even fatalities. Conventional techniques such as chlorination may result in incomplete removal of pathogenic *E. coli*, necessitating the exploration of alternative methods. Thus, removal of *E. coli* by Fenton-like degradation using poly(diallyldimethylammonium chloride) coated iron oxide, PDDA/Fe_3O_4 was investigated in this study. PDDA/Fe_3O_4 was synthesized using co-precipitation method and was characterized using Fourier transformed infrared spectroscopy (FTIR), scanning electron microscopy coupled with energy dispersive X-ray (SEM-EDX), Brunauer-Emmett-Teller method (BET), thermogravimetric analysis (TGA), X-ray diffraction (XRD) and pH drift. The feasibility of PDDA/Fe_3O_4 in the degradation of *E. coli* was also studied. The focus process parameters studied were PDDA/Fe_3O_4 dosage (30 mg and 50 mg) and H_2O_2 concentration (0 mmol/L and 4 mmol/L). In the presence of H_2O_2, 30 mg of PDDA/Fe_3O_4 was found to be sufficient to fully degrade *E. coli* present in water sample through Fenton-like degradation. In the absence of H_2O_2, 50 mg of PDDA/Fe_3O_4 was sufficient to fully remove *E. coli* present in the water sample through adsorption process. It could be concluded that Fenton-like degradation using PDDA/Fe_3O_4 could be a viable alternative for removing *E. coli* in the water treatment process.

TABLE OF CONTENTS

LIST OF TABLES

LIST OF FIGURES

LIST OF SYMBOLS / ABBREVIATIONS

$\bullet O_2H$	hydroperoxyl radicals
$\bullet OH$	hydroxyl radicals
Fe^{2+}	ferrous ions
Fe^{3+}	ferric ions
Fe_3O_4	iron oxide (magenetite)
$FeCl_2 \bullet 4H_2O$	iron (II) chloride tetrahydrate
$FeCl_3 \bullet 6H_2O$	iron (III) chloride hexahydrate
H^+	hydrogen ions
H_2O_2	hydrogen peroxide
H_3O^+	hydronium ions
$H_3O_2^+$	oxonium ions
HCl	hydrochloric acid
NaCl	sodium chloride
NaOH	sodium hydroxide
NH_4OH	ammonia solution
-OH	hydroxyl group
OH^-	hydroxyl ions
PDDA	poly(diallyldimethylammonium chloride)
$PDDA/Fe_3O_4$	poly(diallyldimethylammonium chloride) coated iron oxide
vt %	volume percent
$\gamma\text{-}Fe_3O_4$	maghemite
AOPs	advanced oxidation processes
ATP	adenosine triphosphate
BET	Brunauer-Emmett-Teller method
DAEC	diffusely adherent *E. coli*
E. coli	*Escherichia Coli*
EAEC	enteroaggregative *E. coli*
EHEC	enterohemorrhagic *E. coli*
EIEC	enteroinvasive *E. coli*
EPEC	enteropathogenic *E. coli*
ETEC	enterotoxigenic *E. coli*

FTIR	Fourier-transform infrared spectroscopy
IR	infrared
MNPs	magnetic nanoparticles
NPs	nanoparticles
PDDA	poly(diallyldimethylammonium chloride)
PZC	point of zero charge
SEM-EDX	scanning electron microscopy coupled with energy dispersive X-ray
STEC	Shiga toxin-producing *E. coli*
TGA	thermogravimetric analysis
UPEC	uropathogenic *E. coli*
UV	ultraviolet
XRD	X-ray diffraction

LIST OF APPENDICES

CHAPTER 1

INTRODUCTION

1.1   General Introduction

Water is the most fundamental necessity for all living forms on earth to survive. Among the universe, only earth is capable of supporting life due to readily available stable liquid water bodies on the planet surface. However, life cannot live in the absence of water. Humans use water for daily routines, like bathing, cooking and drinking. Hence, the existence of low-quality water will surely bring a significant impact on humans.

Due to rapid growth of population, industry and agricultural activities, water pollution has become a severe issue in Malaysia. Besides having an adverse impact on the long-term viability of water supplies, water pollution also affects living organisms and plants, as well as the public health and the economy. According to Razelan, Tahir and Yahaya (2018), around 783 million people worldwide were suffering from shortage of clean water. Not to mention, water-related infections had also killed around 6 to 8 million people. In many developing countries like Malaysia, poor water resource management is one of the main factors of water pollution. Without the participation of the government and the public, holistic and integrated approaches to tackle water quality issues will not be able to be carried out. The cost of wastewater treatment is high in terms of building new plants, buying equipment, utilities and labour. This had caused some of the factories which do not have additional funds to discharge used chemicals directly into the river without any treatment. Consequently, more rivers are polluted. The surrounding water and living organisms are also affected in terms of health and cleanliness.

With reference to the data provided by the Malaysia Environmental Quality Report 2016, among the investigated rivers (477 rivers), 10 % were polluted, 43 % were slightly polluted and the remaining 47 % were clean (Chai, 2020). Figure 1.1 shows the Malaysia river water quality trend from 2008 to 2017. The available clean rivers were continuously declining except a small peak in 2011 (59 %) and 2015 (58 %). Furthermore, for the proportion of slightly polluted rivers, it was considered generally rising. Averagely, 10 % of

the rivers were categorised as polluted from 2008 to 2017. However, the high percentage of slightly polluted rivers had a high possibility of becoming polluted in future if there is still no additional effort taken to manage the water resources. In 2016 and 2017, there were only 47 % and 46 % of clean rivers left. This indicated that the accessible clean river water source was not even half of the overall river water.
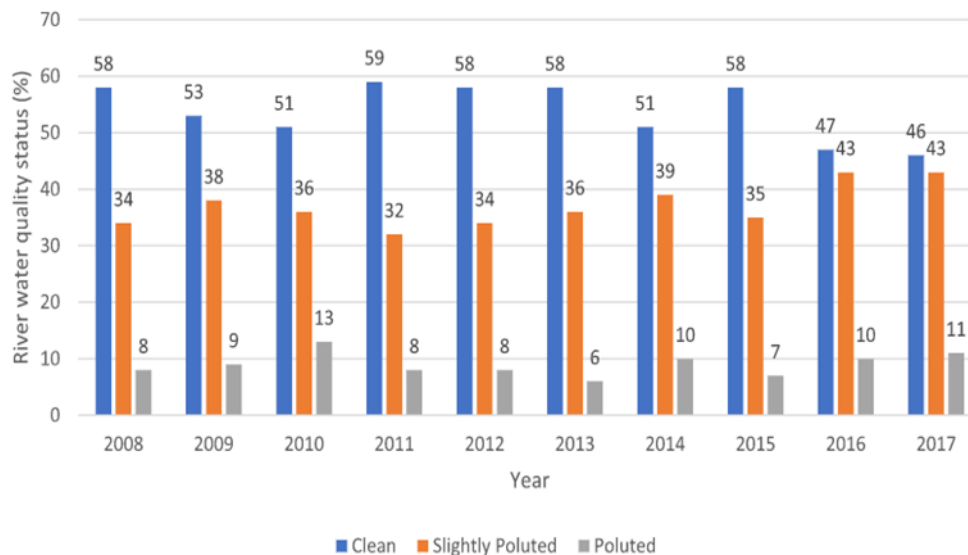
Figure 1.1: Malaysia River Water Quality Trend from 2008 to 2017 (Chai, 2020).

Water pollution originates from point sources and nonpoint sources (Afroz and Rahman, 2017). Pollution from a single, identified source, such as industrial facilities, factories, or sewage treatment plants, is referred to as a point source. Nonpoint source pollution is pollution that does not originate from a single source or point and cannot be traced back to a specific site. Sediments, excess fertilizers and urban runoffs are some of the examples of the non-point source. In 2008, the Department of Engineering had recorded a total of 9,524 sewage treatment plants as water pollution point sources (Afroz et al., 2014). The plant also stand a contribution of 54.1 % from the total detected water pollution point source in Malaysia. Untreated sewage being directly discharged into the river will lead to the degradation of aquatic organisms, later resulting in the disruption of the ecosystem. Moreover, humans that use polluted water for daily activities will also be infected by the water-borne diseases.

Sewage consists of sanitary sewers, combined sewers and storm sewers. Since faeces is the primary source of disease-causing organisms in water, untreated sewage effluent may directly affect the water quality. Thus, faecal bacteria like *Escherichia Coli* (*E. coli*) are widely employed as a water pollution indicator (Price and Wildeboer, 2017). *E. coli* is a bacteria that is commonly found in the warm-blooded organisms' intestine. In general, most of the *E. coli* are harmless and they aid in food digesting. However, some strains, like Shiga toxin-producing *E. coli* (STEC), had resulted in serious foodborne illness such as damaging the human intestine lining (Bertoldi et al., 2018). The transmission of *E. coli* is normally through food, including unpasteurized milk, undercooked ground meat, contaminated water and much more. *E. coli* is chosen as the sewage indicator due to its thermotolerant properties to withstand high temperatures during detection procedure. Fast, affordable, sensitive and easy detection methods were available for *E. coli* (Odonkor and Ampofo, 2013). Although the presence of disease-causing bacteria and pathogens is not always implied by the mere existence of *E. coli*, it serves as a guidance for water quality determination. When high levels of *E. coli* were detected, it indicated that there would be a high possibility of faecal-borne microorganisms like Salmonella to exist (Odonkor and Mahami, 2020).

To improve the water quality, bacteria and pathogens like *E. coli* should be treated. Various treatments could be done to reduce the level of *E. coli* in water. Chlorination is widely utilized due to low cost, simplicity and high efficiency. By adding optimum amount and concentration of chlorine, *E. coli* can be killed and removed. Other methods like ultraviolet (UV) light may also get rid of *E. coli* through the destruction of its DNA. However, these methods possess limitation such as the generation of secondary hazardous waste product in the chlorination method and the high operating cost of UV treatment. On the other hand, Fenton-like degradation is one of the common and more economy feasible treatment methods that could be applied to treat the water sources that are contaminated with microbial pollutants. In Fenton-like degradation, iron oxide (Fe_3O_4) reacts with hydrogen peroxide (H_2O_2) to produce strong oxidising hydroxyl radicals ($\cdot OH$) that can degrade *E. coli* (Wang, 2008).

1.2   Importance of the Study

Water quality in Malaysia is currently deteriorating, owing to rapid urbanization of rural regions, industrial development, and other human activities. Increased sewage production indirectly contributes to the increasing amount of untreated sewage being discharged into rivers or seas. Hence, high concentration of *E. coli* was detected in the polluted river which represents high faecal contamination. To cope with the consequences of *E. coli*, merely using filtration method may not fully get rid of *E. coli*. Thus, Fenton-like approach can be applied to degrade *E. coli* and avoid them from reproducing in the water sample. Furthermore, during the Fenton-like reaction, iron sludge may be produced which affects the *E. coli* degradation efficiency. Through the application of heterogeneous Fenton-like reaction, this problem may be overcome. In addition, Fe_3O_4 used in the Fenton-like degradation are nanoparticles where it may be unstable during the reaction. Hence, by having a poly(diallyldimethylammonium chloride) (PDDA) coat, the Fe_3O_4 are more stable and able to achieve high efficiency of the *E. coli* degradation process.

1.3   Problem Statement

Various *E. coli* removal techniques have been developed to cope with the severe faecal contamination of water supply. However, conventional techniques like chlorination may not completely get rid of *E. coli* from water samples. Studies conducted by McCrary et al. (2013) explained that *E. coli* in the wastewater effluent was merely harmed by chlorine during the disinfection process. Hence, when *E. coli* was placed in an ideal and suitable water conditions, it might regrow and proliferate. Incomplete degradation of *E. coli* may bring harmful effects to human health and contaminate the water supply. *E. coli* will cause abdominal pain, diarrhea and kidney disease to humans. Drinking water supply was one of the carriers of *E. coli* which will transmit to humans when water was consumed. In short, Fenton-like degradation of *E. coli* is the best way to minimize the risk of humans getting bacterial infection.

Homogeneous Fenton-like reaction will cause the formation of iron sludge where additional treatments are required. At the end of the reaction, iron ions must be precipitated out of the system which is costly in terms of labour, reagents and time (Deng et al., 2008). To be safely released, the effluent must

be neutralised with a base. Large volumes of sludge were generated during neutralisation, which is a significant restriction of the process owing to the disposal issues. The Fenton process had obvious downsides such as expended acid, base, and produced sludge. In fortune, the creation of heterogeneous systems had promoted Fenton chemistry that may function at near neutral pH and having benefits such as no requirement for acid or base, no sludge production, and the ability to recycle the promoter (Costa et al., 2006). Therefore, a possible solution to this issue is replacing homogeneous Fenton-like reaction with heterogeneous Fenton-like reaction.

The naked Fe_3O_4 tended to agglomerate due to the weak Van der Waals force (Gosens et al., 2010). Consequently, the iron particle size would increase, followed by the reduction of total surface area. Thus, the available active sites for reaction also decreased, leading to an ineffective *E. coli* degradation process. Integration of polymeric materials would alter the chemical functionality and surface charges of the naked Fe_3O_4 (Duran et al., 2008). Moreover, the polymeric coating also reduced agglomeration in aqueous environments and provided possible interaction with different contaminants for the adsorption process. In a nutshell, coating Fe_3O_4 with PDDA may be a possible solution to reduce agglomeration and achieve a high degradation efficiency.

1.4 Aim and Objectives

The aim of this study was to investigate the degradation of *E. coli* via Fenton-like degradation process using poly(diallyldimethylammonium chloride) coated iron oxide (PDDA/Fe_3O_4). In order to achieve the aim of study, the following main objectives were listed:

1. To synthesis the poly(diallyldimethylammonium chloride) coated iron oxide.
2. To characterize the poly(diallyldimethylammonium chloride) coated iron oxide.
3. To investigate the feasibility of poly(diallyldimethylammonium chloride) coated iron oxide in the degradation of *E. coli* via Fenton-like degradation.

1.5   Scope and Limitation of the Study

The research focussed on the Fenton-like degradation of *E. coli* using PDDA/Fe_3O_4 catalyst. PDDA/Fe_3O_4 nanoparticles (NPs) was synthesized using co-precipitation method. A mixture of ferric ions (Fe^{3+}), ferrous ions (Fe^{2+}), PDDA solution, deionized water and ammonia solution was heated under constant stirring. After washing process, magnetic separation was utilized for the filter of PDDA/Fe_3O_4 NPs from the resulting effluent.

Next, characteristics of PDDA/Fe_3O_4 were studied by utilizing analytical instruments including Fourier-transformed infrared spectroscopy (FTIR), scanning electron microscopy coupled with energy dispersive X-ray (SEM-EDX), Brunauer-Emmett-Teller method (BET), thermogravimetric analysis (TGA), X-ray diffraction (XRD) and pH drift method. The chemical and physical properties of PDDA/Fe_3O_4 such as functional groups, surface morphology, specific surface area, thermal stability, crystalline structure and surface charge were studied.

Furthermore, the feasibility of PDDA/Fe_3O_4 NPs in the degradation of *E. coli* via Fenton-like degradation was investigated. The focus parameters are PDDA/Fe_3O_4 NPs dosage and H_2O_2 dosage. The final solution after degradation was cultivated in agar plate for cell count to check the concentration of *E. coli* left in the solution.

In fact, besides PDDA/Fe_3O_4 NPs dosage and H_2O_2 dosage, other parameters such as pH and contact time also affects the degradation efficiency of *E. coli* via Fenton-like degradation. However, these parameters are not investigated in this study.

CHAPTER 2

LITERATURE REVIEW

2.1   *E. coli*

E. coli is a bacterium which originated from the Enterobacteriaceae family under Gammaproteobacteria class (Jang et al., 2017). *E. coli* is a Gram-negative adaptable rod-shaped bacterium that is easily found and vulnerable to both natural and random genetic alterations. In general, *E. coli* was commonly found in humans and other warm-blooded species' large intestines. There was a significant collection of sequenced E. coli genomes that demonstrate size and genomic diversity variations between commensals and pathogens, revealing a wide range of variation within the same bacterial species.

2.1.1   Classification of *E. coli*

E. coli is made up of pathogenic and non-pathogenic bacteria. Non-pathogenic *E. coli* can act as commensals and are naturally present in the gut microbiota of humans and many other animals. For pathogenic *E. coli*, they are classified as extraintestinal and diarrheagenic pathogens, with numerous pathotypes and spontaneous hybrid strains. Among the pathogenic *E. coli*, they might be facultative or obligate. Facultative refers to the ability to exist in more than one distinct environmental situation whereas obligate means limited to a specific trait. When facultative *E. coli* were not in their natural habitat, they could act as opportunistic pathogens, causing a range of extraintestinal diseases. In contrast, infections caused by intestinal obligatory pathogenic mutations occurred in a range of conditions, ranging from mild diarrhoea to potentially lethal illnesses (Braz, Melchior and Moreira, 2020).

Under the pathogenic category, *E. coli* that cause diarrheagenic diseases is known as diarrheagenic *E. coli*. Diarrheagenic *E. coli* strains can be further classified into six pathotypes. Firstly, enteropathogenic *E. coli* (EPEC) was a prevalent cause of watery diarrhoea in newborns as well as intermittent diarrheal outbreaks. Other symptoms might also include fever, vomiting, dehydration and lethargy. Moreover, EPEC might occasionally induce bloody diarrhoea as an effect of colonization of ileum (Liu, 2014). EPEC infections

were linked with a unique intestinal histopathology characterized as 'attaching and effacing', in which the bacteria attached to intestinal epithelial cells and induced severe cytoskeletal alterations. Diarrhoea was most likely caused by mechanisms such as active ion secretion, intestinal inflammation, increased intestinal permeability, and a reduction in absorptive surface area due to microvillus effacement (Kaper, Nataro and Mobley, 2004).

Enterotoxigenic *E. coli* (ETEC) possessed similar infections with EPEC and it is known as traveler's diarrhoea. ETEC infections were spread via the faecal-oral route and were often acquired by contaminated food and water. Food left uncovered, table-top sauces and street food are examples of high-risk items contaminated with etiological agents for traveler's diarrhoea. Furthermore, surface water might contain ETEC and could be a significant cause of illness when in contact. Beginning with a fast onset of watery faeces and vomiting, the illness might advance to dry mouth, quick pulse and lowered blood pressure due to gradual fluid and electrolyte loss (Liu, 2014). However, the diarrhoea would last for just 3 to 4 days. In addition, ETEC caused sickness by colonizing the small intestine and attaching to the host epithelial lining via surface proteins termed CFs. Adherent ETEC then produced enterotoxins, which generate the clinical symptoms associated with ETEC-induced diarrhoea (Croxen et al., 2013).

Enterohemorrhagic *E. coli* (EHEC) often causes hemorrhagic colitis, which was characterized by bloody stools and intestinal ulcerations. Unlike EPEC, EHEC does not cause fever but mostly bloody diarrhoea. In roughly 10 % of patients, EHEC O157 infection could cause haemolytic uraemic syndrome (HUS), which is characterized by abrupt renal failure, hemolytic anaemia and thrombocytopenia (Shah et al., 2018). EHEC strains, like EPEC strains, are attached to mucosal cells but in the colon by actin reorganisation. These strains generated Shiga-like toxins, which have receptors on intestinal cells and in the kidney that could cause HUS (Katouli, 2010).

Clinical symptoms of enteroaggregative *E. coli* (EAEC) infection include watery diarrhoea, stomach discomfort, vomiting and nausea. EAEC could induce both acute and chronic diarrhoea which lasts more than 14 days. Malnourished hosts might be unable to heal mucosal damage, making them susceptible to chronic or recurrent diarrhoea (Liu, 2014). The invasion

mechanism is where EAEC colonized the intestinal mucosa, generating a thick layer of auto-aggregating bacteria that promotes long-term colonization and contributes to malnutrition. In terms of the presence of potential virulence genes, this pathotype was variable and had lately been subdivided into conventional and atypical EAEC (Girao et al., 2006).

Enteroinvasive *E. coli* (EIEC) is biochemically, genetically, and pathogenetically linked to *Shigella spp*. EIEC produced invasive inflammatory colitis with watery diarrhoea, comparable to other E. coli pathotypes and Shigella spp. In severe cases, dysenteric faeces might contain blood and mucous. There was also the possibility of fever and severe cramps. Like Shigella, EIEC might infiltrate intestinal epithelial cells, most notably in the large intestine (Liu, 2014). EIEC was the sole invasive pathotype which entered epithelial cells in an endocytic vesicle followed by endocytic vacuole dissolution and intracellular multiplication. These strains lysed vesicles inside cells and then migrated across the cytoplasm to neighbouring epithelial cells. Bloody diarrhoea was caused by the active invasion of intestinal cells (Katouli, 2010).

Diffusely adherent *E. coli* (DAEC) is a recently studied pathotype that has been found to cause chronic watery diarrhoea in both adults and children. From 18 months to 5 years of age, the relative risk of diarrhoea depends on the surging of DAEC. Among six types of diarrheagenic *E. coli*, DAEC distinguished themselves from others by exhibiting a specific adhesion behaviour on Hep-2 cells (Liu, 2014). Nevertheless, there were limited studies and research on the mechanism of DAEC. Generally, in a diffuse adhesion pattern, DAEC attached themselves to the small bowel (Katouli, 2014). Besides, DAEC strains caused a cytopathic effect, which was characterized by the formation of lengthy cellular extensions that wrapped around adhering bacteria (Kaper, Nataro and Mobley, 2004).

Apart from diarrheagenic *E. coli*, Uropathogenic *E. coli* (UPEC) is an *E. coli* strain that causes urinary tract infection (UTI) and has distinct virulence genes from other strains. These strains were typically derived from faeces and induce UTI by colonizing the vaginal introitus and the periurethral region before entering the urinary system. They might then climb to the bladder, causing cystitis, or to the kidney, causing pyelonephritis, which could lead to renal failure and death if not treated (Katouli, 2014).

2.1.2 *E. coli* in Malaysia

According to Utusan Malaysia, the tests done by an independent microbiology lab identified traces of the *E. coli* bacterium in Sungai Kim Kim which is located in Johor Bahru. Moreover, according to the Malay daily, measurements indicated that *E. coli* in up to 410,000 CFU/100mL was found in the water samples of Kim Kim river. However, the standard threshold for the recreational park water bodies was only 1,000 CFU/100mL. Thus, the National Water Quality Standard had sorted the river in the lowest Class V of readings (Chin, 2021). The existence of high level of *E. coli* indicated high degree of contamination in the river. If contacted with the highly polluted water, skin itchiness may happen. Besides, a low level of total dissolved oxygen was detected due to the oxygen consumption by *E. coli* bacterium. Consequently, aquatic life was threatened.

EHEC is one of the most prevalent zoonotic agents that may be transferred from animals to people and is a leading cause of severe illness and death in food-borne outbreaks. The EHEC serotype O157:H7 is critical among pathogenic *E. coli* because of its devastating consequences in humans and its rising documented incidence in various locations throughout the world, particularly the Japan and United States (Shah et al., 2018). As a result, the majority of *E. coli* investigations conducted in Malaysia focused mostly on the serotype O157:H7. Table 2.1 summarizes research conducted in Malaysia on the prevalence of *E. coli* and its harmful strains in various samples.

Table 2.1: Prevalance of *E. coli* and Its Pathogenic Strains in Various Samples in Malaysia.

Sample Type	Findings	Reference
Ducks' intestines, wash water, faeces and soil in duck farms and wet markets	Samples collected from ducks' intestines, wash water, faeces and soil in duck farms and wet markets had an *E. coli* presence at 82 %, 50 %, 88 %, and 72 %, with an overall incidence of 79 % of *E. coli* and 29 % of total samples positive for *E. coli* 0157:H7.	Zaliha and Rusli (2004)

Table 2.1: Continued

Samples	Findings	Reference
Raw cattle milk	In Peninsular Malaysia, 930 raw cow milk samples were gathered from 360 randomly selected dairy milk farmers. *E. coli* was found in 64.5 % (600) of the samples, whereas *E. coli* O157:H7 was found in 33.5 % (312) of the milk samples.	Chye, Abdullah and Ayob (2004)
Beef	The laboratory of Food Science and Biotechnology of Universiti Putra Malaysia provided 20 bacterial strains recovered from beef samples. 76 % of the 14 bacterial strains tested positive for *E. coli* 0157:H7 after being collected from four separate supermarkets in Selangor and the Federal Territory of Malaysia.	Sahilah et al. (2010)
Water and sediments from rivers	Water and sediment samples were taken from 64 distinct sites, mostly along the Sangga Besar, Sepetang, and Selinsing Rivers on Malaysia's northwest coast. *E. coli* was found in 85 % (148) of the 175 presumptive *E. coli* isolates recovered from water and sediment samples collected at eight separate locations. All samples tested negative for EPEC, EHEC, ETEC, DAEC, and EIEC, with the exception of two EAEC isolates. All 15 antibiotics tested were found to be resistant in 20 (14 %) E. coli isolates.	Ghaderpour et al. (2015)
Food samples	176 Escherichia coli isolates were found in various food items collected in Selangor, Malaysia, including cattle beef (61), buffalo meat (28), chicken (18), lamb (18), pegaga (17), selom (17), ulam raja (11), tenggek burung (5), and belacan (1). 47.7 % (84) of the isolates tested positive for *E. coli* O157.	Cheah et al. (2015)

2.2   Removal of *E. coli*

Several approaches were studied to clean wastewater effluent because the presence of *E. coli* was highly undesirable. The removal methods of *E. coli* could be categorised as non-destructive and destructive approaches.

2.2.1   Non-destructive Method

Non-destructive method refers to the removal techniques that do not kill or cause damage to the cell or substances. The mechanism of these techniques is mostly filtration based. Membrane filtration and adsorption are some of the examples of non-destructive methods.

Membrane filtration process is about the retention of cultivated bacteria by a filter with specific media. It is a lab scale test where the *E. coli* in water samples were quantified after filtration for further analysis. Suspended particles and bacteria are originally present in the feed and drain. To avoid additional host bacteria intermixing, these water samples were processed with filtering using a cellulose nitrate sterile membrane filter with 0.45 μm pore size. The plaque forming technique was used to measure the filtered solution. As the suspended solid remaining on the filter includes target phage, 3 % beef extract was used to elute it. The eluted solution was then filtered again with a 0.45 μm filter to eliminate any remaining bacteria (Otaki, Yano and Ohgaki, 1998). Membrane filtration, on the other hand, had several limits. Samples having a high turbidity but a low *E. Coli* content might induce filter clogging, necessitating a lengthy filtration period (Vergine et al., 2017).

Adsorption is a physical process that involves the attachment of soluble molecules (adsorbate) to the surface of a solid substrate (adsorbent). Adsorbents must have a large surface area to allow more attachment of molecules and thus removing them from the water sample. Activated alumina, activated carbon and resins were some of the examples of adsorbents (Samer, 2015). Due to its high adsorption rates, high chemical stability and the ability to reduce the concentration of harmful microorganisms, activated carbon had been widely employed in point-of-use filtering systems. According to Burchacka et al. (2021), the activated carbon had a large surface area where 1 g of it could have around 3000 m^2 area. This was contributed by the well-developed microporosity which was less than 2 nm of pore size. Activated carbon could adsorb Gram-

negative bacteria including *E. coli*. However, the adsorption capacity was directly influenced by the macropores available in the activated carbon. The fundamental disadvantage of activated carbon was their high biocompatibility with microorganisms. During the purifying process, bacteria might multiply on carbon, leading the carbon compounds themselves to become contaminants (Pal, Joardar and Song, 2008). Fortunately, by implying adsorption mechanism, Upadhyayula et al. (2008) stated that single-walled carbon nanotubes had antibacterial characteristics that allow them to efficiently concentrate and destroy microorganisms in polluted water. When bacteria contacted with nanotubes, they entered the cell membrane, disturbed its activities, and finally killed the cell's viability. It was believed that the cylindrical form of nanotube fibres, together with a high aspect ratio, was primarily responsible for bacterial cell death. When compared to granular or powdered adsorbents, fibrous media usually had a higher surface area for bacterial adsorption. Moreover, an increase in the aspect ratio would results in a larger surface area. Besides, single-walled carbon nanotubes with greater than 2000 of aspect ratios were predicted to absorb microorganisms effectively.

2.2.2 Destructive Method

Destructive method refers to the removal of *E. coli* by damaging or killing the bacterium cell. Chlorination, UV radiation and advanced oxidation processes (AOPs) are some of the examples of destructive methods.

Chlorination is the most common chemical treatment of microorganisms, especially *E. coli*. Chlorine is a powerful oxidant and able to become an alternative for disinfection due to its simplicity of handling and low initial cost. Chlorination inactivates bacteria by causing membrane permeability damage, which was followed by adenosine triphosphate (ATP) release, the presence of lesions in mRNA and DNA, and the ultimate oxidation of extracellular ATP (Xu et al., 2018). However, the development of odours and off-tastes, as well as the probable formation of disinfection by-products like trihalomethanes had limited the usage of chlorine. Research had shown that *E. coli* was susceptible to chlorine. According to a study conducted by Owoseni, Olaniran and Okoh (2017), exposure to free chlorine and total chlorine at concentration of 1.1 mg/L and 1.2 mg/L respectively for only one minute

resulted in a significant reduction of pathogenic strains of *E. coli* 0157:H7. Similarly, with a 0.2 mg/L of free chlorine concentration and a contact period of 0.5 min, higher than 99.9 % inactivation of *E. coli* was obtained. However, investigations by Osuolale and Okoh (2015) had shown that *E. coli* might survive in chlorinated effluents. Studies had found a high link between low chlorine residuals and *E. coli* survival. In the Eastern Cape of South Africa, for instance, recovery of *E. coli* bacteria happened in the wastewater effluents with low chlorine residuals which vary between 0.05 and 0.25 mg/L.

UV radiation is frequently employed in medical facilities to disinfect tools and apparatus. Harmful microorganisms like *E. coli* have to be eliminated to protect humans from diseases. The sun, xenon lamps and mercury pressure lamps are some of the UV light sources (Onkundi Nyangaresi, Zhang and Shen, 2020). Long-term exposure to UV light could modify a cell's genetic material, resulting in mutations and lastly cell death. UV wavelength between 200 and 300 nm were favoured by the adsorption of DNA molecules (Zimmmer and Slawson, 2002). The adsorption of UV photons by the cell would result in damage of its DNA molecule. The change of nucleotide base pairing, the formation of new bonds between similar adjacent nucleotides and the alteration in cell's genetic material would lead to the halt of DNA replication due to the dimerization effect (Kodoth and Jones, 2015). Studies by Vermeulen et al. (2007) had concluded that the most effective UV light wavelength in killing *E. coli* was 265 nm, with a LD_{100} of 1.17 log mJ/cm^2. LD_{100}, which refers to the lethal dose or the dose of radiation that required to cause a 100 % death of the exposed population, was achieved at this wavelength by effectively destroying all chemical bonds in the cell samples. Short wavelength UV was found to break strong P-O, O-H, and N-H bonds or form energetic free radicals, resulting in greatest damage to cells. A part of the backbone structure of nucleic acids are P-O bonds, while O-H and N-H bonds are required for the hydrogen bonds that keep proteins and DNA in their tertiary structure. The loss of resonance and the exponential rise in UV absorption by water at wavelengths less than 265 nm were the primary reasons for the reduced lethality and less uniform lethal dosage across the sample.

Moreover, AOPs like ozonation, Fenton process and photocatalytic process could effectively treat *E. coli* in wastewater. AOPs utilizes highly

reactive oxygen species to oxidise and break down wide range of contaminants. For instance, ozone is widely known for its high oxidising ability and inactivation of microorganisms such as bacteria and viruses. One of the primary benefits of ozonation is that the gas leaves no identifiable residues, since ozone decomposes quickly into oxygen, unlike other common sanitizers such as chlorine. Ozone has no unpleasant chemical taste or odour when dissolved in water, and it will not irritate human skin when in contact. Moreover, as ozone is a highly flammable gas, it was manufactured and utilized on-site where no storage tank is needed (Prabakaran et al., 2012). Ozone also could not be over-dosed as the unused ozone will escape from the water and revert to oxygen. Hence, the ozone treatment process would be cheaper compared to other disinfection methods like UV radiation. Besides, the oxidation reactions were thousands of times faster than chlorine for the destruction of microorganisms and it could treat all water-borne pathogens in appropriate doses which could not be done by chlorine (Hajiali and Pirumyan, 2018). Ozone derived its antibacterial by interacting with organic functional groups in bacteria's cellular wall. To begin, the ozone interacted with the unsaturated bonds in the membrane-bound phospholipids and lipopolysaccharides on the bacterial cell's surface. When disruption happened on the membrane's permeability and structural integrity, the cell interior was exposed to the external environment, causing the happening of cell lysis (Spit et al., 2022). As *E. coli* which is a Gram-negative bacterium, having a structure of thin peptidoglycan lamella covered by an outer membrane consisting of polysaccharides and lipoproteins, it was said to be more vulnerable to ozone treatment (Wani et al., 2015).

2.3 Fenton-like Degradation

AOPs are alternative destructive removal methods for *E. coli* which able to operate under ambient temperature and pressure. AOPs could drive oxidation processes by using the high reactivity of •OH. •OH could be created in situ using one or a combination of chemical oxidation methods such as ozone and H_2O_2, with or without the assistance of radiation sources such as ultrasounds and UV. Moreover, •OH might be created in a more advanced procedure using gamma radiation, microwaves and the ferrate reagent (Soon and Hameed, 2011). Table 2.2 shows the standard reduction potential of common oxidants. •OH which was

having up to +2.80 V oxidation potential, was the second most powerful oxidant after fluorine, reacting 10^6 - 10^{12} times quicker than ozone depending on the substrate to be destroyed. Theoretically, higher oxidation potential favors the reaction, resulting in higher efficiency. However, fluorine was not considered as the oxidising agent of AOPs as it has too strong oxidising ability. Thus, •OH was chosen and it was believed that it would be able to degrade pathogens include *E. coli* in AOPs.

Table 2.2: Standard Reduction Potential of Common Oxidants (Babuponnusami and Muthukumar, 2014).

Oxidant	Oxidation Potential (V)
Fluorine (F_2)	3.03
Hydroxyl radical (•OH)	2.80
Atomic oxygen (O)	2.42
Ozone (O_3)	2.07
Hydrogen peroxide (H_2O_2)	1.77
Potassium permanganate ($KMnO_4$)	1.67
Chlorine dioxide (ClO_2)	1.50
Hypochlorous acid (HClO)	1.49
Chlorine (Cl_2)	1.36
Oxygen (O_2)	1.23
Bromine (Br_2)	1.09

The Fenton reaction, which uses Fe^{2+} ions as the catalyst and H_2O_2 as the oxidant, is one of the most often utilized AOPs. Fenton reaction offered various benefits, including high performance and simplicity for organic oxidation, as well as non-toxicity where H_2O_2 could be degraded into ecologically friendly species such as water and oxygen thus leaving no harmful residue (Wang et al., 2016). Other than Fenton reaction, there was also a similar reaction where Fe^{2+} ions were replaced by Fe^{3+} ions which named as Fenton-like reaction. Clearly, the Fenton and Fenton-like reactions were inextricably linked. Fe^{2+} ions catalysed Fenton reaction while Fe^{3+} ions, the product of Fenton process, catalysed Fenton-like reaction (Jiang et al., 2013).

Table 2.3 shows the reactions equations for Fenton and Fenton-like reactions (Babuponnusami and Muthukumar, 2014). Equation 2.1 refers to the Fenton reaction where the Fe^{2+} ions were oxidised into Fe^{3+} ions in order to breakdown H_2O_2 into •OH. It was commonly regarded as the heart of Fenton chemistry. Equation 2.2 is the Fenton-like reaction where the produced Fe^{3+} ions could be reduced by interacting with excess hydrogen peroxide to yield Fe^{2+} ions and additional radicals. Fenton-like reaction was slower compared to Fenton reaction and it permitted Fe^{2+} ions regeneration in a cyclic manner. Apart from Fe^{2+} ions regeneration, hydroperoxyl radicals (•O_2H) were also generated. •O_2H might target organic pollutants as well, although they were less sensitive than •OH. Furthermore, since H_2O_2 was consumed and Fe^{2+} ions were regenerated from Fe^{3+} ions through these reactions, Equation 2.2 to 2.5 reflected the rate limiting processes in Fenton chemistry. Other than that, Equation 2.6 to 2.9, which were radical-radical reactions or hydrogen peroxide-radical reactions, had also been found to occur during the Fenton process.

Table 2.3: Reactions and Rate Constants for Fenton and Fenton-like Reactions (Babuponnusami and Muthukumar, 2014).

Reactions	Rate Constants $(L\ mol^{-1}\ s^{-1})$	Equation Label
$Fe^{2+} + H_2O_2 \rightarrow Fe^{3+} + OH^- + \cdot OH$	$40 - 80$	2.1
$Fe^{3+} + H_2O_2 \rightarrow Fe^{2+} + \cdot O_2H + H^+$	9.1×10^{-7}	2.2
$Fe^{2+} + \cdot OH \rightarrow Fe^{3+} + OH^-$	$2.5 - 5 \times 10^8$	2.3
$Fe^{2+} + \cdot O_2H \rightarrow Fe^{3+} + HO_2^-$	$0.72 - 1.5 \times 10^6$	2.4
$Fe^{3+} + \cdot O_2H \rightarrow Fe^{2+} + O_2 + H^+$	$0.33 - 2.1 \times 10^6$	2.5
$\cdot OH + \cdot OH \rightarrow H_2O_2$	$5 - 8 \times 10^9$	2.6
$\cdot OH + H_2O_2 \rightarrow \cdot O_2H + H_2O$	$1.7 - 4.5 \times 10^7$	2.7
$\cdot O_2H + \cdot O_2H \rightarrow H_2O_2 + O_2$	$0.8 - 2.2 \times 10^6$	2.8
$\cdot OH + \cdot O_2H \rightarrow H_2O + O_2$	1.4×10^{10}	2.9

Both of the Fenton and Fenton-like reaction uses iron ions as a catalyst. This was due to iron ions would possess active site to allow decomposition of H_2O_2 molecules into •OH (Soon and Hameed, 2011). Furthermore, iron would

oxidise Fe^{2+} ions to Fe^{3+} ions and then reduced back to Fe^{2+} ions during the Fenton and Fenton-like process (Wang, Liu and Sun, 2012). Catalysis processes were categorised based on the phase of catalyst utilized. Hence, Fenton chemistry could be divided into two types which are homogeneous and heterogeneous processes.

2.3.1   Homogeneous Process

In homogeneous process, the interaction type between the Fenton's reagent and the chemicals to be removed is mainly focused on. According to the Haber-Weiss method, •OH for AOPs could be generated in a solution containing dissolved iron and H_2O_2 (Rusevova, Kopinke and Georgi, 2012). Fenton reaction uses Fe^{2+} ions or Fe^{3+} ions as catalyst to aid in the decomposition of H_2O_2 into strong oxidising •OH. As the reaction time increases, the more Fe^{2+} ions would be consumed (Nidheesh, 2015). Hence, a large amount of Fe^{2+} ions were needed where the legal threshold of the permitted iron concentration presents the effluent was normally exceeded. An example of the catalyst applied in homogeneous Fenton reaction was iron(II) salts which dissolved in acid medium (Garrido-Ramirez, Theng and Mora, 2010). Catalysis reaction occurred not only on the liquid surface but in the entire liquid body (Wang et al., 2016). Furthermore, due of its homogeneous catalytic nature, homogeneous Fenton reaction solely involved chemical change and had no mass transfer constraint (Wang, 2008). The chemical changes that occurred in the homogeneous phase were exclusively determined by the nature of the reacting chemicals' interactions with the molecules to be destroyed (Soon and Hameed, 2011).

The mechanism of homogeneous Fenton process was proposed by Bouasla, Ismail and Samar (2012) which shown in Figure 2.1. Homogeneous Fenton process possessed complex mechanism. In detail, •OH were produced through the chain initiation reaction which shown in Equation 2.1. Nevertheless, in Equation 2.3, Equation 2.7 and Equation 2.9, Fe^{2+} ions, H_2O_2 and $•O_2H$ would scavenge •OH by self-oxidising into Fe^{3+} ions. It was also possible that the •OH would auto-scavenged which depicts in Equation 2.6. Furthermore, H_2O_2 had the ability to become both radical generator and scavenger (Babuponnusami and Muthukumar, 2014).
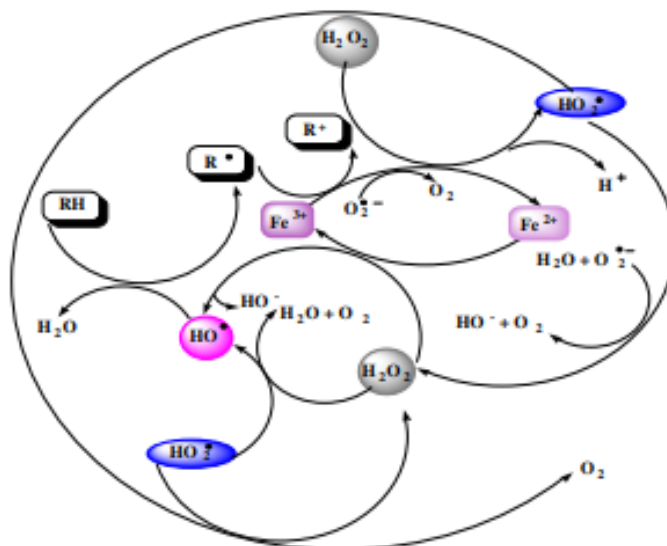
Figure 2.1: Mechanism of Homogeneous Fenton and Fenton-like Oxidation of Organic Compounds (Bouasla, Ismail and Samar, 2012).

Homogeneous Fenton reaction normally operated in acidic conditions with low pH which was around pH 2.8 to 3.0 (Jain et al., 2018). This optimum pH condition was attributable mostly to the presence of larger quantities of Fe^{3+} ions and Fe^{2+} ions in the solution when compared to other pH levels. Metal solubility would also be affected by the pH of the solution. For instance, Fe^{3+} ions were added into a pH 3 solution in the form of hexa-aqua ferric complex, $[Fe(H_2O)_6]^{3+}$. This ferric complex was hydrolysed further, forming additional complexes such as $[Fe(H_2O)_5OH]^{2+}$ and $[Fe(H_2O)_4(OH)_2]^+$. In these complexes, the Fe^{3+} ions and ligands attraction was greater than that between ligands and Fe^{3+} ions in $[Fe(H_2O)_6]^{3+}$. The concentration of complexes other than $[Fe(H_2O)_6]^{3+}$ increased when the pH rose above 3. As a result, as pH increases, the usable percentage of Fe^{3+} ions for the Fenton reaction declines (Nidheesh, 2015).

Furthermore, a pH 3 condition was to ensure that the iron exists in the solution as photo-active species, consisting a portion as $Fe(III)(OH)^{2+}$ and the rest as Fe^{3+} ions. When a lower pH is used, protons would scavenge •OH, causing the concentration of $Fe(III)(OH)^{2+}$ to decrease. As the Fenton reaction was slow, Fe^{3+} ions and •OH increased with time. Thus, when a higher pH was used, Fe^{3+} ions would be precipitated as an oxyhydroxide (Garrido-Ramirez,

Theng and Mora, 2010). Iron sludge production could be reduced by increasing the rate of Fe^{2+} regeneration and maintaining the pH at 3.

Most of the wastewater were alkaline or neutral. To maintain the Fenton reaction at a pH 3 condition, a large volume of acid needed to be added into the reaction medium (Nidheesh, 2015). About using Fenton reaction to clean the water source in situ, it was said to be difficult as if acid is added for pH correction, additional cost would be needed and there was a high possibility that undesirable product would be formed, causing the need of further treatment. In contrast, if no pH correction being done, a large volume of iron sludges would be generated which resulted in disposal and environmental issues. These iron sludges would be dried and sent to landfill where no catalyst regeneration was allowed (Domingues et al., 2018). As a result of large volume of iron sludges being produced, treatment of downstream was required to raise the effluent's pH, precipitate and settle down the catalyst for separation process. Nevertheless, the settled ferric hydroxide was not easy to be separated from the solution because of the colloidal characteristics of the resulting dispersion (Araujo et al., 2011).

2.3.2   Heterogeneous Process

Heterogeneous process was introduced to overcome the disadvantages and limitations of homogeneous Fenton reaction. It was suspected that the dissolved iron which act as the catalyst was driving the formation of iron sludge. Hence, a new approach where a solid catalyst was used to replace the dissolved iron had proposed. There were some requirements of the solid catalyst which to be utilized, including high efficiency in removal, able to withstand long period, low leaching and effective in wide range of pH and temperatures. Some of the examples of heterogeneous catalyst were iron oxide minerals, mesoporous materials and zeolites (Rusevova, Kopinke and Georgi, 2012).

Catalyst reaction of heterogeneous process occurred on the surface of the catalyst. It was said that the position of catalysis was significant in determining the processes of diffusion and adsorption of H_2O_2 and other reactants (Wang et al., 2016). The mechanism of heterogeneous Fenton reaction in deactivating bacteria in Figure 2.2 was proposed by Thomas, Dionysiou and Pillai (2021). Furthermore, chemical equations of heterogeneous process also

discovered by Kwan and Voelker (2003). Equation 2.10 depicted the reaction between the surface Fe^{2+} ions and H_2O_2 to produce surface Fe^{3+} ions, •OH and hydroxyl ions (OH^-). Then, a $Fe^{3+}(H_2O_2)$ complex would be formed in Equation 2.11 as a result of reacting surface Fe^{3+} ions with H_2O_2. For Equation 2.12, it was about the decomposition of $Fe^{3+}(H_2O_2)$ complex to generate surface Fe^{2+} ion, •O_2H and hydrogen ions (H^+).

$$Fe_{surface}^{2+} + H_2O_2 \rightarrow Fe_{surface}^{3+} + \cdot OH + OH^- \qquad (2.10)$$

$$Fe_{surface}^{3+} + H_2O_2 \rightarrow Fe_{surface}^{3+}(H_2O_2) \qquad (2.21)$$

$$Fe_{surface}^{3+}(H_2O_2) \rightarrow Fe_{surface}^{2+} + \cdot O_2H + H^+ \qquad (2.32)$$
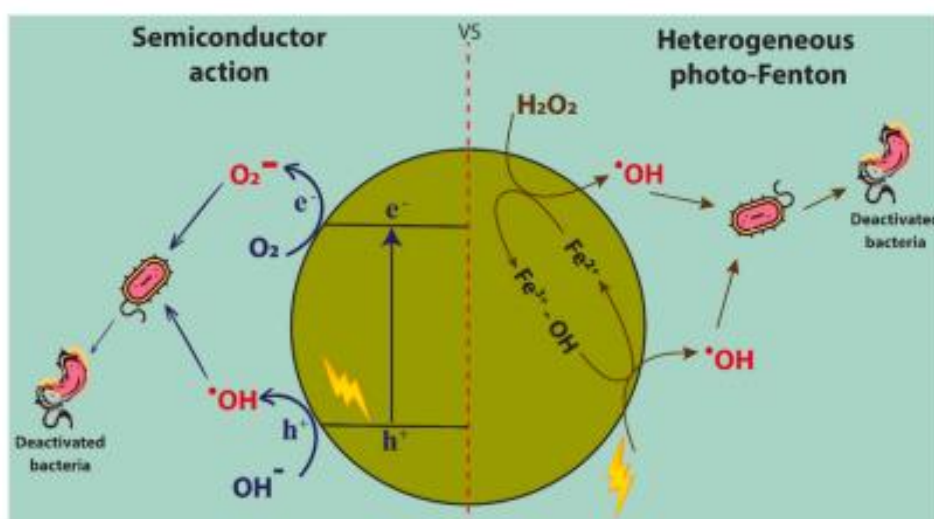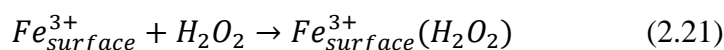
Figure 2.2: Mechanism of Heterogeneous Fenton Reaction on Deactivation of Bacteria (Thomas, Dionysiou and Pillai, 2021).

In heterogeneous reaction, there were physical changes which occurred on the surface of the catalyst and chemical changes which happened at the active spots of reactants. In the active sites, mass transfer limiting adsorption occurred. After the reaction, the desorption of products would result in the availability of active sites for absorption of the new reactants. Hence, the surface features and pore structure of the solid catalyst would bring a significant impact on the efficiency, kinetic rate, and stability in the solid catalysed Fenton reaction (Soon and Hameed, 2011).

Unlike homogeneous process, heterogeneous solid catalyst could operate Fenton reaction under wide pH range. This was due to the immobilization process occurred on the structure and interlayer space of Fe(III) catalyst. Consequently, the catalyst was still capable in producing •OH from H_2O_2, and the precipitation of iron hydroxide was avoided. Aside from exhibiting reduced iron ion leaching, the heterogeneous catalysts were also able to be recover easily at the end of reaction and they were still active for the following reactions (Garrido-Ramirez, Theng and Mora, 2010). Nidheesh (2015) also supported that the metal ion leaching from the catalyst was minimal. As sludge formation was driven by the leaching rate, only a little sludge production was found in heterogeneous process. Thus, no additional sludge treatment would be required. The relatively low leaching characteristics also resulted in minimal amount of iron species being consumed in a heterogeneous Fenton reaction. In short, the catalysts were easily separated at the end of reaction.

2.3.3   Comparison of Homogeneous and Heterogeneous Process

Table 2.4 shows the comparison of both homogeneous and heterogeneous Fenton reaction in various aspects.

Table 2.4: Comparison of Homogeneous and Heterogeneous Fenton Reaction.

Aspects	Homogeneous Process	Heterogeneous Process
Site of reaction	Entire liquid body	Surface of catalyst
Mechanism	Chemical reaction takes place solely	Chemical reaction, physical adsorption and desorption
pH	Narrow acidic pH range, adjustment of pH is required.	Wide range of pH
Sludge production	Large amount of iron sludge were produced	Insignificant sludge production, depending on the metal leaching properties of catalyst

Table 2.4:   Continued

Aspects	Homogeneous Process	Heterogeneous Process
Downstream treatment	Require	Not require
Catalyst loss	High, the amount of Fe^{2+} ions consumed increases with time	Low, minimal amount of iron species being consumed

2.4   Iron Oxide Magnetic Nanoparticles

NPs are a broad range of materials that comprise overall dimensions of less than 100 nm (Murthy, 2007). These materials could be in the shape of 0D, 1D, 2D, or 3D depending on the overall form. NPs had become significant when the effect of particle size on a substance's physiochemical qualities was discovered. There were three layers in NPs which are the surface, the core and the shell. For the NPs surface, it consists of wide range of metal ions, small molecules, polymers and surfactants. The core was the center part of the NPs which was generally known as the NPs itself. Moreover, the shell was said to be chemically distinct from the core in every aspect. Application of NPs on wastewater treatment was widely seen nowadays which contributed by the high surface to mass ratio as well as the features of NPs like special affinity for the adsorption and degradation of both organic and inorganic pollutants (Khan, Saeed and Khan, 2019).

Under NPs, there were magnetic nanoparticles (MNPs) which referred to particles that react to external magnetic fields and having size ranging from 1 to 200nm. Magnetite (Fe_3O_4) or maghemite (γ-Fe_3O_4) were commonly utilized to produce the core of magnetic iron oxide NPs (Lakshmanan, 2013). MNPs could be synthesized through several methods including hydrothermal synthesis, co-precipitation, thermal decomposition and so on. Co-precipitation approach was often applied in the industry by reacting metal oxides with oxidising agents to produce spherical magnetite particles. It was a readily replicable, convenient and straightforward method. The composition, shape and size of the MNPs were determined by the salts implied, the Fe^{2+}: Fe^{3+} ratio, the operating conditions and the ionic strength. However, this technique brought some disadvantages such as the formation of polydisperse particles, the unstable properties of MNPs

and available possibility to the happening of particles agglomeration (Parekh, 2013).

Usage of MNPs in remediation of water had been studied extensively. Instead of "pump and treat" approach where the groundwater was pump up to the ground for further treatment, in-situ method could now be applied by injecting MNPs into the contaminated ground (Gehrke, Geiser and Somborn-Schulz, 2015). MNPs owned a superparamagnetic characteristic where the particles would be magnetised only when a field was present and no residual magnetization would be left when the field is withdrawn. Hence, the clusterization of particles could be avoided. In addition, MNPs had a large particle magnetic moment because of its high magnetic saturation and susceptibility. Therefore, magnetic particles containing pollutants could be easily removed from the groundwater by an external applied magnetic field and gradient. Furthermore, MNPs were able to efficiently remove specific water contaminants due to its high surface-to-volume ratios (Barasel et al., 2019).

Several researches were done on the application of MNPs on the degradation of microorganisms, particularly *E. coli*. Huang, Wang and Yan (2010) concluded that the efficiency of bacteria removal increased with the MNPs concentration until a stabilisation point was achieved. Moreover, bacteria's surface charge and characteristics as well as the hydrophobicity would also affect the efficiency of removal of bacteria from water. Other than that, Pinto et al. (2020) also conducted similar research on the bacteria removal through usage of MNPs. Up to 99.2 % of removal efficiency could be obtained with more than 2 log of reduction for the Gram-negative *E. coli* cells. Besides, the efficiency of *E. coli* removal increased with the contact time until a stabilisation point was achieved. Other authors like Zhang et al. (2018), Rana and Singh (2016) and Zhan et al. (2014) had also discussed upon this application.

2.4.1   Synthesis of PDDA Coated Iron Oxide

Coating of PDDA polymer on Fe_3O_4 NPs is essential in increasing the efficiency in microorganism removal. As stated by Colombo et al. (2012), NPs might have the possibility to flocculate due to the presence of Van der Waals forces whereas MNPs agglomerate due to the magnetic attraction. Hence, surface coating was important to ensure high stability, to target the surface and to reduce the

reticuloendothelial system's response. In addition, coating materials had also some requirements like able to withstand wide range of pH, having attachable functional groups and high ionic strength. Figure 2.3 shows the schematic diagram of the coated MNPs structure (Bull et al., 2014). The biocompatible coating not only ensured a longer shelf life through the protection of the core but also served as a platform for the binding of specific compounds (Parekh, 2013).
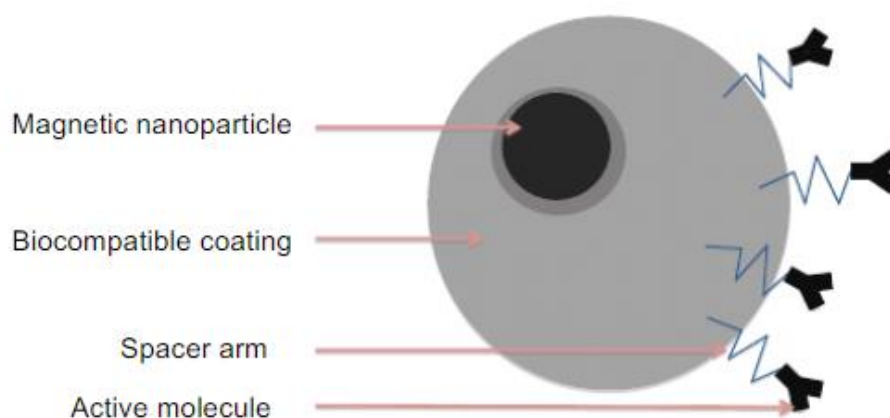
Figure 2.3: Schematic Diagram of the Structure of MNP (Bull et al., 2014).

PDDA was invented by George Butler as a homopolymer in 1957. The structure of PDDA, a water-soluble polymer, is depicted in Figure 2.4 (Rivas, Espinosa and Sanchez, 2018). Its quaternary ammonium functional groups possessed a high charge density where OH^- ions were the charge carriers. Furthermore, the PDDA cyclic structures created significant steric hindrance, preventing the degradation of quaternary ammonium functional groups by S_N2 nucleophilic substitution in an alkaline environment (Samsudin and Hacker, 2019). As a result, PDDA exhibited cohesive, adsorption, and antibacterial capabilities. It was widely employed in a variety of applications, including biological and medical uses as well as wastewater treatment plants (Mevold et al., 2015).

Synthesis of $PDDA/Fe_3O_4$ could be done in various ways. From the method proposed by Azmi et al. (2012), Fe_3O_4 MNPs would be coated by the physisorption of PDDA. A suspension of 1000 ppm Fe_3O_4 MNPs was prepared using deionized water and sonicated so that they are monodispersed. The use of

deionized water was to ensure the absence of impurities that would affect the physisorption process. Likewise, a 0.1667 g/mL PDDA was produced and undergo sonication process. A 24-hour period in a rotator mixer, the pH of both solutions was adjusted to pH 8 so that physisorption of PDDA on Fe_3O_4 MNPs via electrostatic attraction was favourable. The $PDDA/Fe_3O_4$ were then collected and pre-washed before being dispersed in deionized water by using a Nd-FeB permanent magnet.
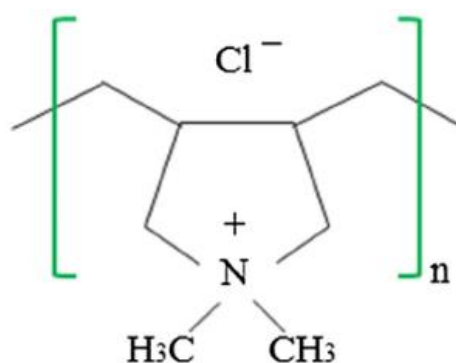
Figure 2.4: Structure of PDDA Polymer (Rivas, Espinosa and Sanchez, 2018).

The second method of $PDDA/Fe_3O_4$ synthesis was proposed by Jang et al. (2018) and Yu et al. (2010). A 20 mL solution which contains 0.8 g of iron (II) chloride tetrahydrate ($FeCl_2 \cdot 4H_2O$), 2.16 g of iron (III) chloride hexahydrate ($FeCl_3 \cdot 6H_2O$) and 1.0 % v/v of PDDA had undergo deoxygenation process through nitrogen gas bubbling for 10 minutes. Then, the oxygen-free solution was passed for heating to 80 °C. Next, a 10 mL of 8M ammonia solution (NH_4OH) was promptly added to the heated solution and left for stirring for 1 hour. Precipitates were formed as the results of the reaction between the heated solution and NH_4OH. After cooling to ambient temperature, the $PDDA/Fe_3O_4$ precipitate were separated using a magnet field. Then, deionized water was used to wash the synthesized $PDDA/Fe_3O_4$ for three times and dried.

In addition, Bogachev et al. (2017) had also done research on the $PDDA/Fe_3O_4$ synthesis method. Fe_3O_4 MNPs which functionalized with a PDDA layer were made by the dispersion of Fe_3O_4 MNPs powder in a PDDA solution with a tenfold mass excess of polyelectrolyte. There were some cleaning equipment used to treat the suspension, including a 2-minute period

treatment for a Sapphir ultrasonic bath, a 45-second period for 4 to 5 times treatment for a submersible ultrasonic disperser and finally a 2-minute period treatment for an ultrasonic bath. The samples were then chilled in an ice bath to minimize the overheating issue during ultrasonication process. Lastly, centrifugation was used to separate the PDDA/Fe$_3$O$_4$ which were subsequently distributed in distilled water.

2.5   Characterization Study

Material characterization study is essential in determining the structure of a material as well as the effect of the structure on its macroscopic characteristic and its performance in technological applications. This study aims to understand the link between physical, chemical and catalytic properties. Wide range of characterization techniques are readily available in the industry. In this study, PDDA/Fe$_3$O$_4$ NPs were characterized by using FTIR, SEM-EDX, BET, TGA, XRD and pH drift.

2.5.1   SEM-EDX

SEM-EDX is an analytical technique that provides information on the morphology and elemental composition of a sample. SEM is an imaging technique that utilizes a beam of electrons to examine the surface of a sample. Electrons interact with atoms which present in the sample to obtain information on the composition and surface topography. Signals would then be created to deliver the information found. A high-quality image would be obtained when the atomic number is high, the backscattering is larger and the electron transmission is lesser (Ortiz Ortega et al., 2022). For EDX, the X-rays emitted would be analysed to detect the element present in the sample. The emission of X-rays were the signals created through the reactions of electron beams and sample atoms (Ellingham, Thompson and Islam, 2017）.

Several studies had been done on the application of SEM-EDX on PDDA coated materials. Among them, Oyehan et al. (2020) had conducted a research on the coating of PDDA polymer on fly ash for the removal of phenol from wastewater. Figure 2.5 shows the SEM images of uncoated fly ash and PDDA coated fly ash. From the image of uncoated fly ash, the fly ash was seen to be having porous structure with pore diameter approximately 2 μm. After the

coating process with PDDA polymer, the morphology of fly ash had some changes in which the surface is smoother, at the same time the pores were also comparably lesser and having smaller pore diameter (approximately 1.1 μm). Besides that, EDX had detected the elemental composition of both uncoated and PDDA coated fly ash. Both samples consist carbon, oxygen and sulphur atoms with similar weight percentage. The element constituents for PDDA polymer like chlorine and nitrogen were not detected by EDX because the contents were below the detection limits.
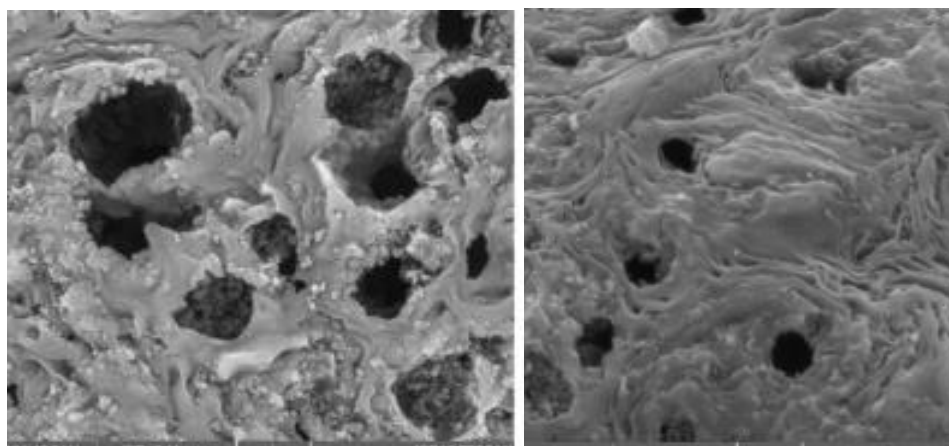
Figure 2.5: SEM Micrographs of Uncoated Fly Ash (Left) and PDDA Coated Fly Ash (Right) (Oyehan et al., 2020).

2.5.2   FTIR

FTIR is an analytical technique used to study the functional groups and molecular bonds present in a material through the application of infrared radiations beam (Ortiz Ortega et al., 2022). Infrared (IR) spectroscopy will determine the absorption of IR radiation by each molecular bond. Then a spectrum would be produced in % transmittance vs wavenumber (cm^{-1}). To determine functional groups in a molecule, it must be IR active. An IR active molecule was one that has a dipole moment. When a material containing an electric dipole was exposed to IR radiation, the molecule absorbed energy and the bond started to oscillate back and forth. As a result, the change in the net dipole moment of the molecule absorbed IR radiation. Furthermore, specific IR radiation would be absorbed by specific molecular bonds at specific wavelength.

No molecules would be having same absorbed infrared spectrum despite having same frequencies (Khan et al., 2018).

Related studies had been done by Jang et al. (2018) on the application of FTIR on PDDA/Fe_3O_4 NPs. In PDDA sample, a strong band at 3440 cm^{-1} was ascribed mostly to the stretching vibration of neither -NR$_3^+$ nor hydroxyl group. whereas the bands at 3000 to 2800 cm^{-1} were attributed to C-H bonding. The existence of a Fe-O bond from Fe_3O_4 was also detected at 539 cm^{-1} in all samples containing Fe_3O_4. Wang, et al. (2015) also detected Fe-O bond at 578 cm^{-1} wavelength through FTIR.

2.5.3   BET

Surface area of PDDA/Fe_3O_4 NPs can be determined by utilization of BET. Assumption made by BET is where adsorption happens by multilayer development, and that at saturation pressure, the number of adsorbed layers is limitless (Walton and Snurr, 2007). The mechanism of BET was about the gas adsorption on the material's surface. Adsorption could be either physically which caused by Van der Waals forces or chemically which caused by a chemical interaction between the adsorbate and the solid. The gas which adsorbed on the adsorbent material was proportional to the material's surface area. Langmuir theory was strongly connected to BET theory. An ideal situation was where only monolayer gas adsorption occurs. As BET theory assumed that all layers are in equilibrium where no interaction would be happening between each layer, the Langmuir equation might be employed for each layer. Molecules which situated in the layers under the initial one functioned as absorption sites for molecules in the above layers (Ambroz, 2018). The calculation approach for BET area was by generating BET plot and determining the monolayer capacity, n_m and thus the specific surface area of the material (Thommes, 2007). According to Jang et al. (2018), the BET specific area obtained for the composite of HPB/PDDA/Fe_3O_4 was 166.16 m^2/g.

2.5.4   XRD

XRD is utilized to study the crystalline structure of samples. The working mechanism could be explained in the way that the exposed X-ray beams would interact with the atoms in the crystal lattice of the sample and resulted in

diffraction scenario. Then, the diffracted rays would be interpreted and a unique diffraction pattern would be produced for each sample. The diffraction pattern consists information about the diffraction peaks' position, intensity, and width. For the peak intensity and width, they provided information about the atomic number and position within the cell. Moreover, the shape and size of a unit cell could be determined through the interpretation of the position of diffraction peaks (Ali, Chiang and Santos, 2021).

Studies on XRD analysis of PDDA/Fe_3O_4 NPs were done by Qu et al. (2015) and Yu et al. (2010). The diffractogram for PDDA/Fe_3O_4 NPs were obtained in the angle range of 20º to 80º at 2θ. Qu et al. (2015) reported that the diffraction peaks observed at 2θ angle of 30.5°, 35.5°, 43.0°, 53.8°, 57.0º and 62.7° corresponded to the crystal planes (220), (311), (400), (422), (511) and (440) of face-centred cubic lattice of Fe_3O_4 NPs. Both naked Fe_3O_4 NPs and PDDA/Fe_3O_4 NPs shared the same XRD patterns which indicated that the coating of PDDA polymer did not disrupt the formation of crystal lattice of Fe_3O_4 NPs.

2.5.5 TGA

TGA functions to measure the changes in the weight of a sample during heating process under controlled conditions. It is often used as an analytical technique to study the thermal stability and the compositions of a material. The commercialized TGA usually operated at temperature up to 1000 ºC with the flow of purge gas such as nitrogen, oxygen and helium. In the heating process, mass loss would be seen in common which refers to those volatile elements, including residual solvents and absorber moisture. Mass gain may also be detected before the starting of degradation process, which was at slow heating rates under oxidising atmosphere. The common heating rate was 3.5 ºC/min, stated by Ortiz Ortega et al. (2022).

Research conducted by Chen, Ju and Chen (2019) reported that the TGA could be performed in the temperature range of 30 to 800 ºC under the heating rate of 5 ºC/min in nitrogen atmosphere. The results revealed that the PDDA/Fe_3O_4 NPs experienced a higher weight loss than Fe_3O_4 NPs which was 92 % and 97 % respectively. From 30 ºC to 150 ºC, the weight loss was suspected as the evaporation of absorbed moisture. For temperature around 200

^{o}C to 470 ^{o}C, the weight loss was referring to the decomposition of PDDA chemical bonds and polymer backbones as reported by Samsudin and Hacker (2019).

2.5.6 pH Drift

Point of zero charge (PZC) referred to the pH value in which the substance's surface net charge is equal to the zero. The PZC indicated that the positive and negative charges were actually having equal amounts. PZC was an essential aspect in characterization of metal oxides. The metal oxides sorption ability could be analysed through PZC which aided in the determination of the probability of harmful ions being attracted by the metal oxides. PZC also varied with type of metal oxides, ranging 6.5 to 1.0 for aluminium oxide, as reported by Mahmood et al. (2011). pH drift was an analytical technique used to determine PZC of the substances. The initial and final pH for each experimental set would be plotted in a graph, followed by the determination of PZC through the intersection point of the curve and the tie line.

The study conducted by Davodi, Jahangiri and Ghorbani (2018) showed the application on pH drift Fe_3O_4 NPs. The PZC for Fe_3O_4 NPs was 6.32. After coating of a positively-charged polymer, named polydopamine, the PZC values decreased to 3.04. The decreased in PZC value might be due to the protonation of amine functional group in the polydopamine. Other than that, the PZC value could be interpreted in the way that the Fe_3O_4 NPs would be positive charge at pH below 6.32 whereas negative charge at pH above 6.32.

2.6 Degradation of *E. coli* by PDDA/Fe_3O_4 NPs

To determine the feasibility of PDDA/Fe_3O_4 NPs in the degradation of *E. coli* via Fenton-like reaction, the reaction conditions must be identified first. Various parameters like PDDA/Fe_3O_4 dosage, H_2O_2 dosage, pH and contact time were reported to have significant impacts to the degradation of *E. coli* through Fenton-like degradation.

2.6.1 Effect of PDDA/Fe_3O_4 NPs Dosage

The PDDA/Fe_3O_4 NPs dosage was an important element in affecting the efficiency of Fenton-like reactions. The system's adsorption and degradation

efficiency increased with the dose of catalyst. It was evident that increasing the PDDA/Fe_3O_4 NPs dosage would increase the pollutant's surface area and adsorption sites. The generation of •OH was dependent on PDDA/Fe_3O_4 NPs dosage. Fe^{3+} ions would be reduced to Fe^{2+} ions then catalysed the decomposition of H_2O_2 to generate •OH for the degradation of *E. coli*. Hence, the increased of PDDA/Fe_3O_4 NPs dosage would ensured the decomposition of H_2O_2 sustained at a high level as more Fe_3O_4 NPs was available for Fenton-like reactions. As a result, with an additional PDDA/Fe_3O_4 catalyst in the system, superior *E. coli* degradation was obtained.

The study of Feng et al. (2019) showed that the increased of catalyst dose increased the inactivation efficiency of *E. coli*. The more the catalyst being fed, the more the active sites readily available for the conversion of H_2O_2 to •OH (Zhao et al., 2015). Thus, high concentration of •OH could be maintained to ensure high efficiency of *E. coli* degradation. Besides, Chen et al. (2020) also reported that increment of Fe^{2+} ions concentration from 0.5 to 1.0 mmol/L boosted the removal efficiency of *E. coli*. Nevertheless, the removal efficiency of *E. coli* showed a drop when the Fe^{2+} ions concentration was increased to 2.0 mmol/L. Theoretically, higher Fe^{2+} ions concentrations resulted in higher reaction rates; but when the Fe^{2+} ions were supplied in excess, it increased in the consumption of H_2O_2 owing to the scavenging effect, which was not beneficial for the •OH generation. Hence, this reflected the situation where the *E. coli* removal efficiency first increased, reached a peak and started to decrease when the Fe^{2+} concentration gradually increased.

2.6.2 Effect of H_2O_2 Dosage

H_2O_2 is a powerful oxidising agent and the amount used will be influencing the total bacteria inactivation rate. In detail, an increased in the dose of H_2O_2 would increase the proportion of bacteria degraded (Babuponnusami and Muthukumar, 2014). Nevertheless, supplying excess H_2O_2 dosage was not encouraged since the leftover H_2O_2 would be contributing to the chemical oxygen demand. An optimal H_2O_2 dosage should be determined because too high H_2O_2 dosage might slow down the degradation rate (Bagal and Gogate, 2014).

Castro-Rios et al. (2017) deduced that a higher H_2O_2 dosage would cause inactivation of *E. coli*. At 0.06 mg/L of H_2O_2 concentration, the

inactivation efficiency of *E. coli* was 38 % whereas at 0.18 mg/L H_2O_2 concentration, the inactivation efficiency of *E. coli* increased up to 56 %. Low inactivation efficiency might be due to the insufficient •OH being generated by H_2O_2. Furthermore, Chaturvedi and Katoch (2019) stated that the *E. coli* removal efficiency increased until a peak and then declined as the H_2O_2 dosage increased. This might be due to the reduced catalytic activity when the concentration of H_2O_2 rose. Similarly, the decreased degradation efficiency was related to the •OH consumption by H_2O_2 to produce $•O_2H$ which shown in Equation 2.6 to 2.8. In contrast, Zhong et al. (2018) proposed a different explanation for the effect of H_2O_2 dosage on the efficiency of *E. coli* degradation. It was believed that the decline of the degradation efficiency in high H_2O_2 amount was solely due to the insufficient time for the reaction to be occurred between the microorganism and •OH which resulted in a self-quenching of •OH.

2.6.3   Effect of pH

The pH condition was critical in Fenton-like degradation process. Xu and Wang (2011) stated that the alteration of pH would directly affect the catalyst and oxidant activity, the dominating iron species, as well as the H_2O_2 stability. In general, the optimal pH for the conventional Fenton reaction was about 2.8 to 3.0. However, the implied of heterogeneous Fe_3O_4 catalysts had offered a wide range of pH which was around 3.0 to 7.0 for the Fenton-like reaction.

  E. coli degradation rates were higher in acidic circumstances because H_2O_2 and Fe^{2+} ions were more stable in the pH range of 3 to 4. According to Bagal and Gogate (2014), at low pH levels like pH 2.5, the degradation efficiency was lower due to the formation of Fe(II) complex which caused the slow reaction between the reactant and H_2O_2 and generating lower concentration of •OH. In addition, the H^+ ions scavenging effect would also contribute to the consumption of •OH which shown in Equation 2.13 (Hassan and Hameed, 2011). At extremely acidic pH, oxonium ion ($H_3O_2^+$) would be form as a result of the capture of a proton by H_2O_2 which shown in Equation 2.14. $H_3O_2^+$ ions would then stabilize H_2O_2 and decrease H_2O_2 reactivity by transforming H_2O_2 to be electrophilic. In contrast, at higher pH levels (pH > 4), the production of Fe(II) complex lowered the synthesis of free radicals, at the same time, the ferric oxyhydroxides precipitate had inhibited the regeneration of Fe^{2+} ions, slowing

the degradation rate. At increased pH, a drop in the •OH oxidation potential had caused the decrease Fenton-like degradation rate (Bagal and Gogate, 2014).

$$\cdot OH + H^+ + e^- \rightarrow H_2O \qquad (2.43)$$

$$H_2O_2 + H^+ \rightarrow H_3O_2^+ \qquad (2.54)$$
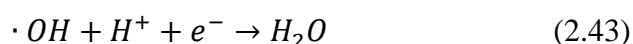
According to Tong et al. (2020), at pH 3.5, a complete *E. coli* degradation was achieved in just 20 minutes with the supply of 5 mM H_2O_2. When the pH was increased to 6.0 and 7.5, around 35 minutes were needed for the complete *E. coli* degradation. Similarly, about 75 minutes were needed when the degradation process was subjected to pH 9.5. Furthermore, Castro-Rios et al. (2017) obtained a 53 % of inactivation efficiency at pH 3.7 but only 39 % at pH 7.3. At pH nearly to neutral, H_2O_2 might be instable which leads to the generation of iron(II) complex thus decreasing the amount of generated •OH for the Fenton-like *E. coli* degradation process. Furthermore, at pH levels around 3 to 4, the Fenton reaction was accelerated, which might enhance the solubility of iron on the catalyst as well as the interaction with H_2O_2, resulting in an improvement in *E. coli* inactivation efficiency.

2.6.4 Effect of Contact Time

As stated by Fajarwati et al. (2020), the collision hypothesis stated that the reaction speed was determined by the number of collisions occurring at the same moment. The more contacts there were, the faster the reaction occurs until the equilibrium conditions were met. The optimal contact time was when the adsorption and desorption rates were in balance. At the start of the degradation process, the degradation rate would increase with the contact duration. Then, a plateau was reached. Because of the high availability of free active sites on the catalyst for the adsorption process, high adsorption rate and degradation efficiency could be obtained. The competition of active sites between H_2O_2 and *E. coli* and also the decreasing of vacant adsorption sites had resulted in the decline of adsorption and degradation rate (Rashed, Eltaher and Adbou, 2017).

Castro-Rios et al. (2017) investigated the effect of contact time on the *E. coli* degradation efficiency. An increase of contact time would increase in the efficiency of inactivation of *E. coli*. For instance, at 50 minutes only 15 %

degradation efficiency achieved but 75 % for a 240 minutes of contact time. Moreover, Tong et al. (2017) discovered that the first 3 hour had a rapid uptake phenomenon and a slight increase until 8 hours. This might due to the saturation of adsorption sites on the catalyst. Besides that, the rapid rate of degradation at first might be attributable to a large number of accessible active sites on the surface of the catalyst. The slower degradation in the last stage was most likely due to decreased accessible active sites (Nuengmatcha et al., 2016).

CHAPTER 3

METHODOLOGY AND WORK PLAN

3.1 Project Workflow

The overall flowchart for this study is presented in Figure 3.1. The initial phase in the research was the synthesis of magnetic $PDDA/Fe_3O_4$ catalyst. One-pot synthesis was achieved by subjecting a mixture of iron precursor and PDDA to heating process under constant stirring for a period of time. The final product was harvested through magnetic separation and drying process. Surface functionalization with PDDA provides stability to the Fe_3O_4 NPs at the same time reducing agglomeration.

Next, the synthesized $PDDA/Fe_3O_4$ NPs was characterized. The morphology and the elemental composition of the $PDDA/Fe_3O_4$ NPs were studied using SEM-EDX. The existence of functional groups on $PDDA/Fe_3O_4$ NPs was then being investigated using FTIR in the frequency range 4,000 - 400 cm^{-1}. Moreover, the surface area of the $PDDA/Fe_3O_4$ NPs was calculated using the BET equation. The crystalline structure was analysed by XRD whereas the thermal stability was studied through TGA. Finally, pH drift was used to determine the PZC of $PDDA/Fe_3O_4$ NPs.

Subsequently, the feasibility of $PDDA/Fe_3O_4$ NPs in the degradation of *E. coli* was investigated. The focus parameters included the dosage of $PDDA/Fe_3O_4$ NPs and the concentration of H_2O_2. The degradation and adsorption efficiency of $PDDA/Fe_3O_4$ NPs was determined by the comparison of initial and final number of *E. coli* colonies in the agar plates.

Step 1: Synthesis of PDDA/Fe$_3$O$_4$ NPs

- Heat the mixture of iron (II) chloride, iron (III) chloride, PDDA and deionized water to 80 ^{o}C.
- Add ammonia solution to precipitate PDDA/Fe$_3$O$_4$ NPs.
- Separate PDDA/Fe$_3$O$_4$ NPs with permanent magnet.

Step 2: Characterization of PDDA/Fe$_3$O$_4$ NPs

- SEM-EDX
- FTIR
- BET
- XRD
- TGA
- pH drift

Step 3: Feasibility Study of PDDA/Fe$_3$O$_4$ NPs in the Degradation of *E. coli*

- Parameters study: PDDA/Fe$_3$O$_4$ dosage and H$_2$O$_2$ concentration
- Adsorption and degradation efficiency of PDDA/Fe$_3$O$_4$ NPs will be determined by comparing the initial and final number of *E. coli* colonies in the agar plates

Figure 3.1: Overall Flowchart of This Research.

3.2   Materials and Equipment

Table 3.1 has listed the materials required in this research. On the other hand, Table 3.2 depicts the equipment needed for this study with their usage being identified.

Table 3.1:   List of Chemicals.

Chemicals	Purity (%)	Brand	Usage
Poly(diallyldimethylammonium chloride) (PDDA)	35	Sigma-Aldrich	Polymer coating for catalyst
Iron (II) chloride tetrahydrate ($FeCl_2 \cdot 4H_2O$)	99.3	Bendosen	Catalyst
Iron (III) chloride hexahydrate ($FeCl_3 \cdot 6H_2O$)	98.4	Bendosen	Catalyst
Ammonia solution (NH_4OH)	30	R&M Chemical	Precipitate catalyst
Hydrochloric acid (HCl)	37	Sigma-Aldrich	pH adjuster
Sodium hydroxide (NaOH)	20	Sigma-Aldrich	pH adjuster
Escherichia Coli (*E. coli*)	-	ATCC	Bacteria source
Sodium chloride (NaCl)	99	Merck	Solvent
Luria broth	-	Condalab	Bacteria cultivation medium
LB agar	-	Condalab	Bacteria cultivation medium
Hydrogen peroxide (H_2O_2)	35	Merck	Oxidant

Table 3.2: List of Equipment.

Equipment	Usage
Scanning electron microscopy coupled with energy dispersive X-ray (SEM-EDX)	To study the morphology and elemental composition of PDDA/Fe_3O_4 and Fe_3O_4 NPs
Fourier transform infrared spectroscopy (FTIR)	To study the functional groups present in PDDA/Fe_3O_4 and Fe_3O_4 NPs
Brunauer-Emmett-Teller (BET)	To study the surface area of PDDA/Fe_3O_4 and Fe_3O_4 NPs
X-ray diffraction (XRD)	To study the crystalline structure of PDDA/Fe_3O_4 and Fe_3O_4 NPs
Thermogravimetric analysis (TGA)	To study the thermal stability of PDDA/Fe_3O_4 and Fe_3O_4 NPs
pH meter	To measure the pH of the solution
Laboratory rotator	To achieve uniform mixing of mixture in pH drift and feasibility study
Autoclave	To sterilize the glassware and apparatus used to handle *E. coli*
Overhead stirrer	To achieve uniform mixing of mixture during the synthesis of PDDA/Fe_3O_4 NPs
Hot plate	To heat up the mixture during the synthesis of PDDA/Fe_3O_4 and Fe_3O_4 NPs
Ultrasound water bath	To isolate the formed PDDA/Fe_3O_4 precipitate from the mixture
Oven	To dry the PDDA/Fe_3O_4 and Fe_3O_4 NPs
Weighing balance	To measure the weight of PDDA/Fe_3O_4 and Fe_3O_4 NPs
Bunsen burner	To sterilize apparatus used to handle *E. coli*
Incubator shaker	To cultivate *E. coli* under controlled conditions

3.3 Synthesis of PDDA/Fe₃O₄ NPs

First, 0.8 g of FeCl$_2$•4H$_2$O and 2.16 g of FeCl$_3$•6H$_2$O were mixed together in 20 mL of deionized water containing 1 vt.% (0.6 mL) PDDA. The solution was heated to 80 °C with constant stirring. Once the temperature reached 80 °C, 10 mL of NH$_4$OH was rapidly added. 1 hour of stirring was allowed for the complete precipitation of PDDA/Fe$_3$O$_4$ NPs. After cooled to room temperature, the formed PDDA/Fe$_3$O$_4$ NPs were isolated with a permanent magnet. Then, deionized water was used to wash the synthesized PDDA/Fe$_3$O$_4$ for three times. During the washing process, sonication was used to completely remove the unreacted raw materials on the NPs. Finally, the PDDA/Fe$_3$O$_4$ NPs were dried overnight in oven at 80 °C and stored in a universal bottle.

3.4 Characterization of PDDA/Fe₃O₄ NPs

Characterization studies like SEM-EDX, FTIR, BET, XRD, TGA and pH drift were conducted on PDDA/Fe$_3$O$_4$ catalyst.

3.4.1 SEM-EDX

SEM analysis was performed on the fresh and spent PDDA/Fe$_3$O$_4$ catalysts as well as naked Fe$_3$O$_4$ NPs in order to analyse their surface morphological structure. Prior to SEM-EDX observation, the catalysts were adhered to the aluminium specimen holder with carbon tape. The samples along with the holder were subjected to a sputter coater to be coated with gold and palladium. Then, the sample holder was inserted into the SEM-EDX equipment and a 15kV of accelerating voltage would be applied. In the process, the samples were scanned by electron beam and the magnified image of the sample with different magnifications were obtained for further analysis. The graph of EDX was also obtained with each peak representing different elements.

3.4.2 FTIR

To determine the functional groups present in the PDDA/Fe$_3$O$_4$ and Fe$_3$O$_4$ samples, the FTIR instrument was used. The sampling technique employed in this study was attenuated total reflectance. FTIR analysis was conducted across 32 cumulative scans for FTIR spectrum ranging from 4,000 to 400 cm^{-1}. The

spectrums acquired were compared to the spectrum in the computer database to identify the specific functional groups.

3.4.3   BET

The degassing process began by placing 0.5 g of the sample into a tube and heating it to 250°C. After degassing, the sample was immersed in liquid nitrogen at a temperature of -196°C to allow for physical adsorption of the nitrogen onto the catalyst sample surface, which allowed for the determination of its specific surface area. The adsorption of nitrogen on the sample also provided information about the pore types, including whether they were mono or multilayered.

3.4.4   XRD

The Cu Kα radiation with 0.15406 nm wavelength was used. The diffractogram for Fe_3O_4 and $PDDA/Fe_3O_4$ NPs were obtained in the angle range of 20° to 80° at 2θ. The scanning rate used was 0.02 s^{-1}. Both of the samples were grounded in prior to ensure that a representative diffraction pattern would be generated. The samples were then be mounted onto a holder, commonly made by low-adsorption material. In the data interpretation process, the acquired graph peaks were compared in the computer database to identify phases present in the samples. By assuming the samples are having spherical shape, Scherrer equation was utilized to calculate the size of crystallite.

3.4.5   TGA

Around 20 mg of powder samples were filled into the crucible. The analysis was carried out in nitrogen atmosphere with a temperature range from 30 to 1000 °C. The heating rate was set at 10 °C/min to prevent the decomposition of pores.

3.4.6   pH Drift

5 centrifuge tubes filled with 25 mL of 0.1 M NaCl solution were prepared. Each centrifuge tubes solution was adjusted to pH 2, 6, 8 and 10 by using either HCl or NaOH solution. Then, 75 mg of samples were measured and added into each centrifuge tubes. The centrifuge tubes were left for mixing in a laboratory rotator for 48 hours under room temperature to ensure equilibrium. After that, the final

pH of each solutions was measured (Stan, 2019). A graph of final pH versus initial pH of the solution were plotted to obtain the PZC value.

3.5 Feasibility Study of PDDA/Fe₃O₄ NPs in the Degradation of *E. coli*

Feasibility study was conducted to determine the ability of PDDA/Fe$_3$O$_4$ NPs in degrading *E. coli* through Fenton-like process. The effect of catalyst dosage and absence of H$_2$O$_2$ were analysed. In this study, there was a total of 4 parts: cultivation of *E. coli*, serial dilution, Fenton-like degradation of *E. coli* and agar spread plate.

3.5.1 Cultivation of *E. coli*

Nutrient broth was prepared as the *E. coli* bacteria's growth medium. In a conical flask filled with 100 mL of distilled water, 3 g of Luria broth powder was added and stirred until completely dissolved. The solution was preheated to approximately 100 ºC before subjected to sterilization process. After covering the mouth of the conical flask with cotton and aluminium foil, the conical flask was placed into an autoclave at 121 °C for 15 minutes. Sterilization process was important as to prevent contamination. When the Luria broth was cooled to room temperature, the *E. coli* was inoculated. The inoculating loop was sterilized by heating until red with Bunsen burner. Then, the mouth of conical flask was sealed with parafilm and left in incubator shaker at 37 ºC for 18 to 20 hours at 100 rpm.

3.5.2 Serial Dilution

Serial dilution was carried out to dilute a solution to a specific concentration for experimental purpose. The approximate numbers of *E. coli* colonies were determined by using standard plate count method. If the agar plate contained more than 300 colonies, it was considered as "too many" which woud affect the colonies counting process. Hence, serial dilution had to be conducted. Firstly, 6 sterile centrifuge tubes were prepared and labelled with appropriate dilution factor. A 9 mL of 0.8 % NaCl solution was added into each centrifuge tubes. After that, 1 mL of cultivated *E. coli* solution was transferred into the first centrifuge tube, indicating the first dilution (10^{-1}). The contents were mixed thoroughly by pipetting up and down. From the first dilution solution (10^{-1}), 1

mL of the solution was pipetted into second centrifuge tube and mixed evenly which indicates the second dilution factor (10^{-2}). The serial dilution process was continued until 10^{-6} dilution was obtained.

3.5.3 Fenton-like Degradation of *E. coli*

A 27 mL of 0.8 % NaCl solution were prepared and poured into a centrifuge tube. 3 mL of the prepared 10^{-6} *E. coli* dilution solution were added into the centrifuge tube and mix thoroughly. Then, 30 mg of PDDA/Fe_3O_4 NPs and 4 mmol/L of H_2O_2 solution were added into the solution. The centrifuge tube was mixed using the laboratory rotator for 4 hours at 70 rpm. Same experimental procedures were repeated by using Fe_3O_4 for comparison to the PDDA/Fe_3O_4 NPs. Table 3.3 shows the data for each experimental set.

Table 3.3: Degradation of *E. coli* Using PDDA/Fe_3O_4 and Fe_3O_4 NPs via Fenton-like Degradation at Room Temperature with a Duration of 4 Hours.

Experimental Set	Catalyst	Catalyst Dosage	H_2O_2 Dosage
1	PDDA/Fe_3O_4	30 mg	4 mmol/L
	Fe_3O_4	30 mg	4 mmol/L
2	PDDA/Fe_3O_4	50 mg	4 mmol/L
	Fe_3O_4	50 mg	4 mmol/L
3	PDDA/Fe_3O_4	50 mg	-
	Fe_3O_4	50 mg	-

3.5.4 Agar Spread Plate

A 17.5 g of LB agar powder was added into a Schott bottle filling with 500 mL of distilled water and stirred until completely dissolved. The solution was preheated to approximately 100 °C before subjecting to sterilization process. The cap of Schott bottle was loosened to prevent overpressure in the container. After that, the conical flask was placed into an autoclave at 121 °C for 15 minutes. When the agar solution was cooled until 50 °C, the agar solution was poured half-filled into each petri dish. The agar plates were left to cool for 15 minutes. Then, the agar plates were kept in inverse direction. The whole agar

solution pouring process was conducted in a laminar flow cabinet to prevent contamination.

After the Fenton-like degradation process, the reacted catalyst was separated from the solution by using a permanent magnet. Then, 0.1 mL of the reacted solution was transferred to the agar plate for the growth of *E. coli*. Agar spread plate was done in a laminar flow cabinet to ensure sterile environment. The transferred solution was spread evenly onto the surface of the agar plate by using a sterile spreader. The spreader was kept sterile by heating with Bunsen burner. However, the heated spreader should not be used immediately instead it should be cooled for approximately 2 minutes to prevent the killing of *E. coli*. Each sample was subjected to 3 agar plates count. All the agar plates were placed in incubator shaker at 37 °C for 20 to 22 hours. The *E. coli* colonies were observed and compared for the determination of degradation efficiency.

CHAPTER 4

RESULTS AND DISCUSSIONS

4.1   Characterization of PDDA/Fe₃O₄ NPs

Several characterization techniques such as SEM-EDX, FTIR, BET, XRD, TGA and pH drift were done on PDDA/Fe_3O_4 NPs. Various aspects like surface morphology, functional group, surface area, crystalline structure, thermal stability and surface charge were studied on the sample tested. Characterization study aimed to analyse the effect of polymer coating on Fe_3O_4 NPs, at the same time proving the success of the coating process.

4.1.1   SEM-EDX

The SEM images of both Fe_3O_4 and PDDA/Fe_3O_4 NPs were analysed to determine the surface morphology of particles. Figure 4.1 (a) and (b) shows the SEM image of both Fe_3O_4 samples at a magnification of ×3,000. The Fe_3O_4 NPs were found to be having irregular shape with uneven sizes. Uneven grinding with a mortar and pestle after the powder synthesis process could result in inconsistent particle size of the Fe_3O_4 NPs. From both SEM images, the polymer coating process did not have a significant impact on the surface structures of the NPs. The surface of NPs was said to be quite smooth but having some smaller particles adhering on it. Moreover, no obvious holes or large pores were found on the PDDA/Fe_3O_4 sample which indicated that the polymer coating process did not destruct the surface of NPs.

Figure 4.2 (a) and (b) show SEM images of both Fe_3O_4 samples at a magnification of ×10,000. At a higher magnification, it could be observed that PDDA/Fe_3O_4 NPs had a smoother surface compared to uncoated Fe_3O_4 NPs. Clusters of NPs adhered to the surface of naked Fe_3O_4, and agglomeration was more apparent in uncoated samples where particle distances were smaller. This phenomenon was due to the magnetostatics coupling between the particles, reported by Rahmawati et al. (2017). PDDA coating reduced agglomeration in Fe_3O_4 NPs due to the introduction of positive charges on the surface, which increased electrostatic repulsion and reduced magnetic attraction between unstable MNPs. The reduced agglomeration in PDDA/Fe_3O_4 NPs suggested that

PDDA coating could improve their stability and dispersibility. In short, SEM images showed the success of PDDA coating on Fe$_3$O$_4$ NPs.
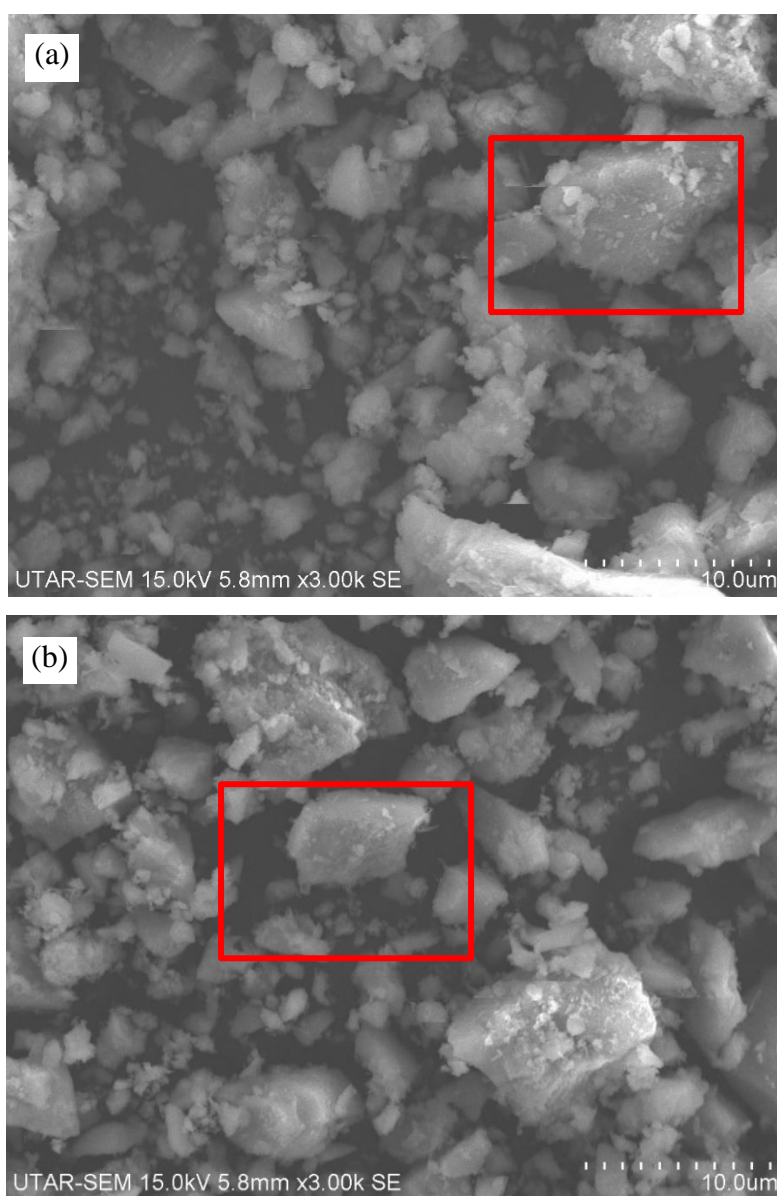

Figure 4.1: SEM Image at ×3.00k Magnification of (a) Fe$_3$O$_4$ NPs and (b) PDDA/Fe$_3$O$_4$ NPs.

EDX spectra and the elemental compositions of both samples are illustrated in Figure 4.3. Both samples contained iron (Fe) and oxygen (O) elements, confirming the existence of Fe$_3$O$_4$ NPs. Notably, the naked Fe$_3$O$_4$ sample exhibitied a detectable amount of chlorine (Cl) at 1.69 % which shown in Figure 4.3(a). The presence of Cl might be due to an insufficient washing process, which could cause leftover unreacted iron chlorides during the

synthesis process. Consequently, the chloride ions might deposit on the NPs surface, resulting in impure Fe_3O_4. Figure 4.3(b) shows that Cl was not detected but carbon (C) at 9.12 % and nitrogen (N) at 2.26 % were present. Referring to the chemical structure of PDDA in Figure 2.4, PDDA was made up of carbon, hydrogen, nitrogen and chlorine atoms. As EDX was not able to detect hydrogen, the remaining elements should be observable. However, Cl did not appear in the graph peaks as the amount of Cl was below the detection limit, similar to the findings of Oyehan et al. (2020). The presence of C and N in $PDDA/Fe_3O_4$ sample were sufficient to confirm the success of the polymer coating process.
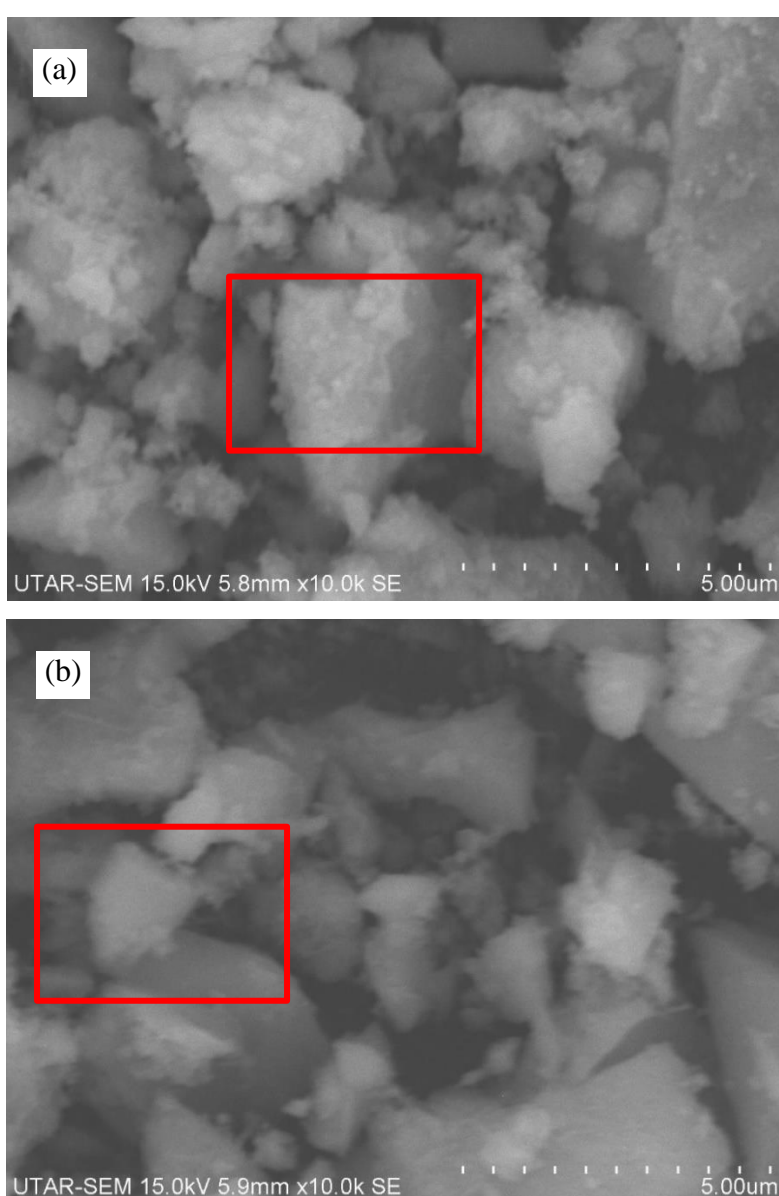

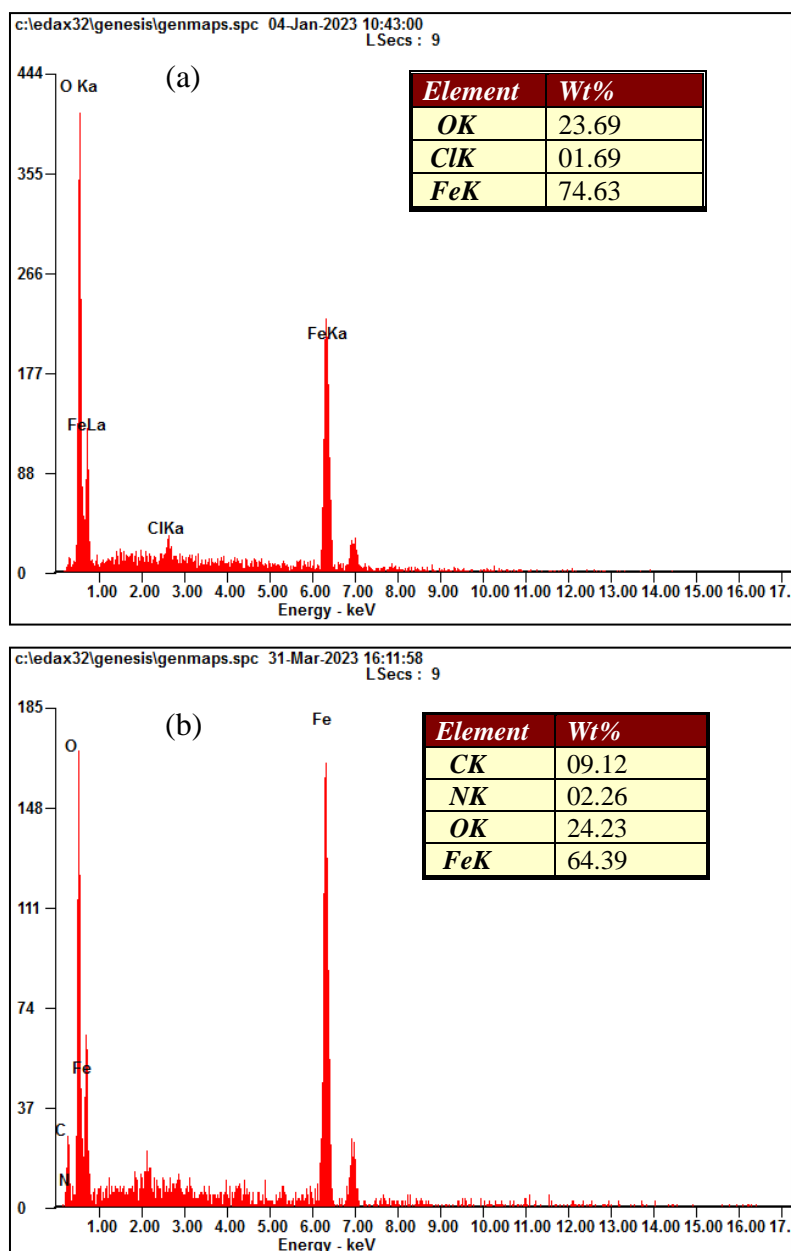Figure 4.2: SEM Image at ×10.0k Magnification of (a) Fe_3O_4 NPs and (b) $PDDA/Fe_3O_4$ NPs.

c:\edax32\genesis\genmaps.spc 04-Jan-2023 10:43:00
LSecs : 9

(a)

Element	Wt%
OK	23.69
ClK	01.69
FeK	74.63

c:\edax32\genesis\genmaps.spc 31-Mar-2023 16:11:58
LSecs : 9

(b)

Element	Wt%
CK	09.12
NK	02.26
OK	24.23
FeK	64.39

Figure 4.3: EDX Spectra and Elemental Composition of (a) Fe_3O_4 NPs and (b) PDDA/Fe_3O_4 NPs.

4.1.2   FTIR

FTIR was used to analyse the functional group exists in both PDDA/Fe_3O_4 and Fe_3O_4 NPs. A graph of transmittance against wavenumber was plotted. All peaks were identified and compared with computer database as well as journal article to identify the indicating functional group.

Figure 4.4(a) shows the FTIR spectra of Fe_3O_4 NPs before coating with PDDA polymer. A broad band appeared at 3313 cm^{-1} was due to the stretching vibration of O-H hydroxyl groups (Jang et al., 2018). This indicated the presence

of moisture in the Fe_3O_4 NPs. Since Fe_3O_4 NPs were prepared in aqueous solution, the bare and unreacted Fe and O atoms situated on the surface tended to bind with OH^- ions and H^+ ions respectively, resulting in a high hydroxyl group (-OH) surface of Fe_3O_4 NPs (Yusoff, Salimi and Jamlos, 2017). To further support, the characteristic band appearing on 1629 cm^{-1} was attributed to the H-O-H bending of hydroxyl group which refers to the water molecules (Jang et al., 2018). For the peaks at about 620 cm^{-1} and 541 cm^{-1}, they were assigned to the stretching vibration mode correlated to Fe-O bonds in the Fe_3O_4 crystalline lattice (Nalbandian, et al., 2016).
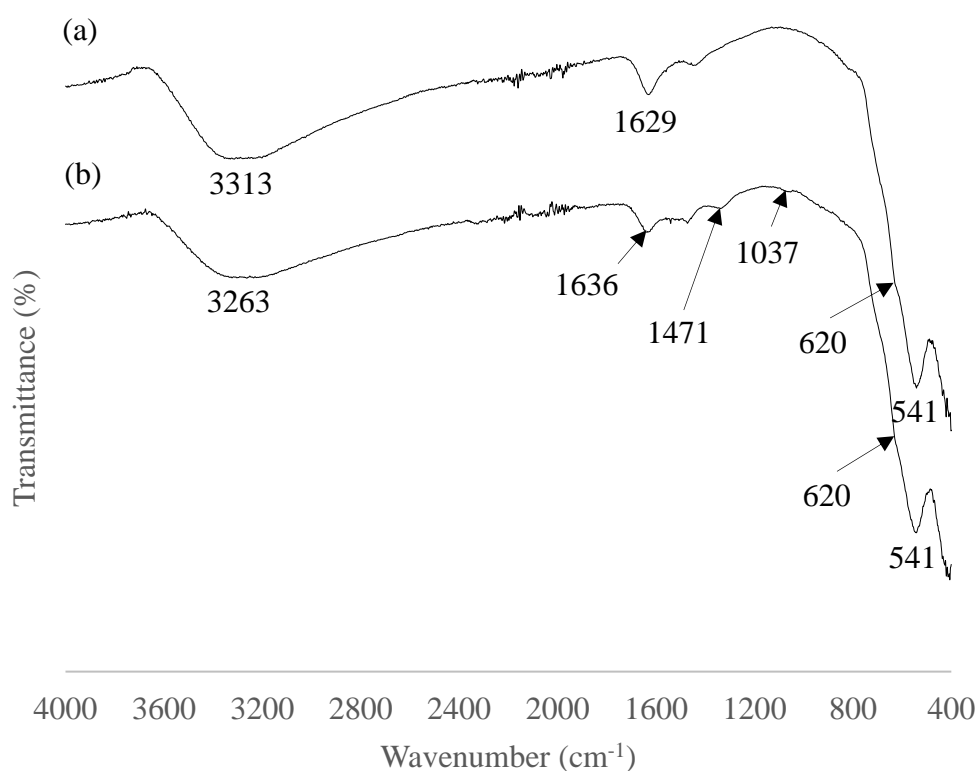

Figure 4.4: FTIR Spectra of (a) Fe_3O_4 NPs and (b) PDDA/Fe_3O_4 NPs.

Figure 4.4(b) shows the FTIR spectra for PDDA/Fe_3O_4 NPs. The presence of new band at 1471 cm^{-1} and 1037 cm^{-1} had proved the success of PDDA polymer coating process. Similar to Fe_3O_4 NPs, moisture was also detected in the FTIR spectra by obtaining vibration bands at around 3263 cm^{-1} and 1636 cm^{-1}. The slight shifting of peaks was due to complex and electrostatic interaction occurring between the reaction of PDDA and Fe_3O_4 during co-precipitation process. The new adsorption peak at about 1471 cm^{-1} was

contributed by vibration bands of C=C group which present in PDDA polymer (Chen, Ju and Chen, 2019). Furthermore, the other new characteristic bands at 1037 cm^{-1} indicated that PDDA polymer was also made up of C-N groups (Lv, et al., 2022). The existence of both C=C and C-N groups could be identified through the chemical structure of PDDA presented in Figure 2.4. In addition, the presence of Fe_3O_4 was detected at vibration bands around 620 cm^{-1} and 541 cm^{-1}. The graph peaks for both samples are summarized in Table 4.1 along with their assignment.

Table 4.1:   FTIR Spectra Assignment of Fe_3O_4 and $PDDA/Fe_3O_4$ NPs.

| Peak Frequency (cm^{-1})			Assignment
Literature	Fe_3O_4	$PDDA/Fe_3O_4$	
3375	3313	3263	O-H stretching
1615	1629	1636	H-O-H bending
1470	-	1471	C=C
1099	-	1037	C-N
630	620	620	Fe-O
580	541	541	Fe-O

4.1.3   BET

Surface area is an important factor that affects the efficiency of the *E. coli* degradation process. The pore structure details of both $PDDA/Fe_3O_4$ and Fe_3O_4 samples are presented in Table 4.2. Similar to the findings of Chen, Ju and Chen (2019), the PDDA coating process increasesd the specific surface area and decreased the average pore diameter of Fe_3O_4 NPs. The specific surface area of Fe_3O_4 NPs increased by 5 times after the surface functionalization with PDDA polymer. This was attributed to the introduction of a layer of positive charges by PDDA on the surface of NPs, resulting in an increase in electrostatic repulsion between them. This, in turn, prevented agglomeration and allowed for a greater exposure of the surface area. As for the average pore diameter, the reduction might be due to the deposition of PDDA onto the pores, which fill them up. The coating process had an overall effect of increasing the adsorption capacity which was beneficial for the removal in *E. coli* during water treatment process.

Table 4.2: Pore Structure of Fe_3O_4 and $PDDA/Fe_3O_4$ NPs.

Sample	Specific Surface Area (m²/g)	Average Pore Diameter (nm)
Fe_3O_4	34.05	16.54
$PDDA/Fe_3O_4$	164.68	5.37

4.1.4   XRD

The crystal structures of Fe_3O_4 and $PDDA/Fe_3O_4$ NPs were examined using XRD measurement. There was a total of 6 characteristic peaks obtained at $2\theta =$ 30.54°, 35.74°, 43.58°, 54.08°, 57.25° and 62.86°. From Figure 4.5(a) and (b), both Fe_3O_4 and $PDDA/Fe_3O_4$ NPs resulted in similar XRD diffraction pattern. This proved that the crystalline structure of Fe_3O_4 NPs remained unchanged after the PDDA polymer coating process. As reported by Qu et al. (2015), the 6 diffraction peaks at 2θ angle of 30.54°, 35.74°, 43.58°, 54.08°, 57.25° and 62.86° corresponded to the crystal planes (2 2 0), (3 1 1), (4 0 0), (4 2 2), (5 1 1) and (4 4 0) of the face-centred cubic lattice of Fe_3O_4 NPs. In addition, the diffraction pattern of Fe_3O_4 sample showed a few unlabelled small peaks, indicating incomplete and inhomogeneous crystal growth (Siregar, et al., 2020). Besides, these small peaks were attributed to the impurities present in the sample. Conversely, from Figure 4(b), the presence of impurities was less apparent. Therefore, it is recommended to coat Fe_3O_4 NPs with PDDA polymer, as it did not perturb the formation of crystal lattice of Fe_3O_4 NPs.
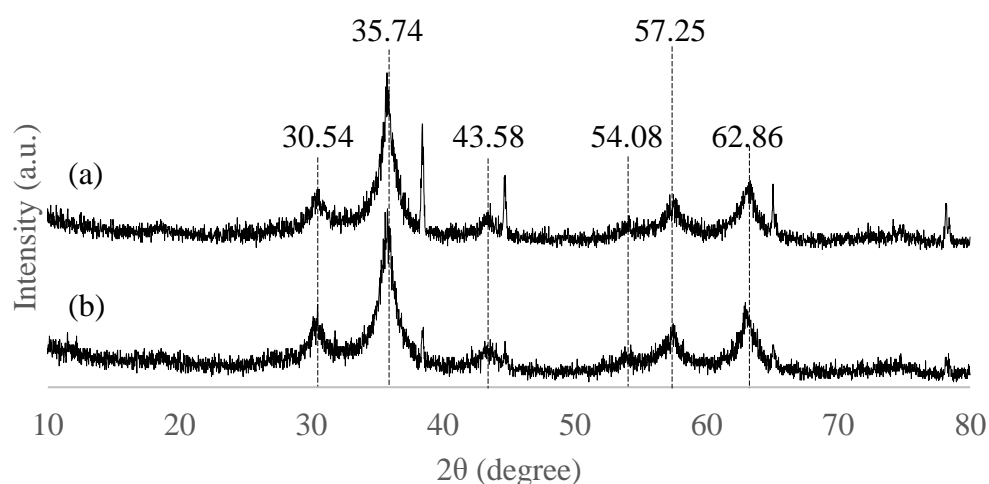
Figure 4.5: XRD Results of (a) Fe_3O_4 NPs and (b) $PDDA/Fe_3O_4$ NPs.

4.1.5 TGA

The thermal stability of both Fe_3O_4 and $PDDA/Fe_3O_4$ NPs were studied through analysis of TGA results. The obtained TGA results were plotted as a graph of weight loss versus temperature. Figure 4.6(a) illustrates the weight loss curve of uncoated Fe_3O_4 NPs. The absolute weight loss for Fe_3O_4 sample was 13.6 % over the entire temperature range. Between 0 °C to 150 °C, the weight loss was caused by the evaporation of physically and chemically adsorbed water. Subsequently, the weight loss beyond 200 °C was due to the decomposition of the organic components located on the surface (Chen, Ju and Chen, 2019). The uncoated Fe_3O_4 NPs were deemed unstable as weight loss was still evident even after removing all moisture.
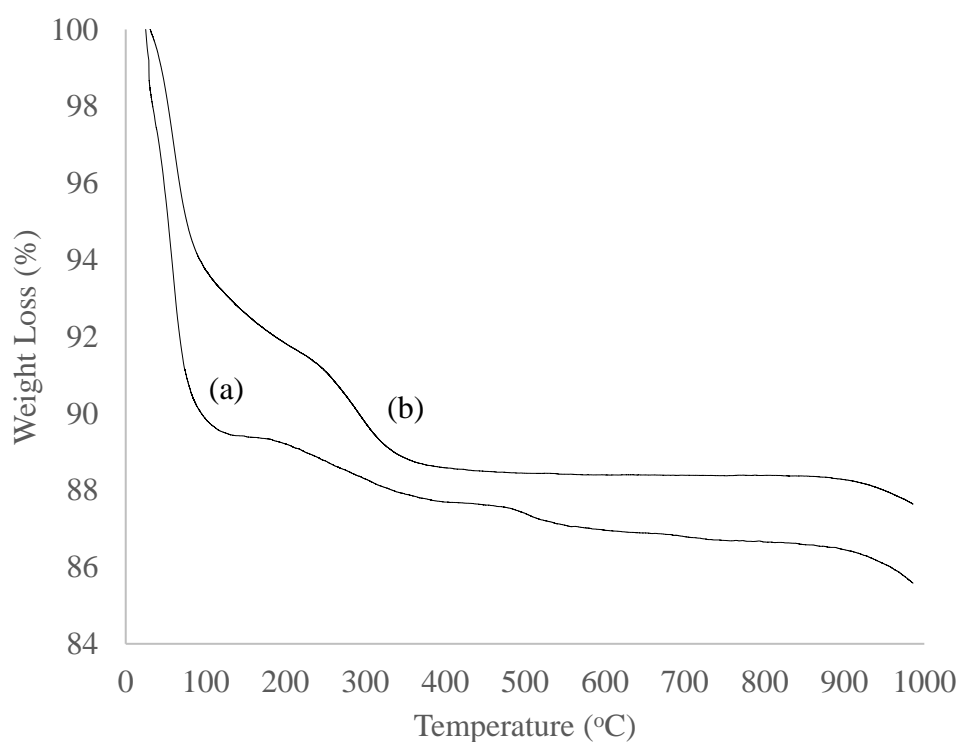

Figure 4.6: TGA Curves of (a) Fe_3O_4 NPs and (b) $PDDA/Fe_3O_4$ NPs.

After coating Fe_3O_4 NPs with PDDA polymer, the overall weight loss decreased to 12.5 %. The thermal decomposition of $PDDA/Fe_3O_4$ NPs was observed in three stages, occurring at approximately 0 - 100 °C, 100 – 250 °C and 250 – 400 °C. As reported by Zhou et al. (2019), the first stage was attributed to the release of adsorbed moisture present in the sample. The second stage was due to the decomposition of quaternary ammonium cationic structure and cross-

linking bridges of PDDA. In addition, the breakdown of C-C bonds in PDDA also contributed to the observed weight loss. The weight loss observed in the third stage, ranging from 250 $^{\circ}$C to 400 $^{\circ}$C, was due to the destruction of PDDA polymer backbones. Weight loss beyond 400 $^{\circ}$C was not obvious, indicating that the decomposition of organic components in Fe$_3$O$_4$ NPs was not significant. Hence, the decomposition of PDDA was said to be ranging from 100 $^{\circ}$C to 400 $^{\circ}$C. In short, functionalization of PDDA increased the thermal stability of Fe$_3$O$_4$ NPs.

4.1.6   pH Drift

The PZC and surface charge of both samples were determined through pH drift analytical method. The pH drift results were plotted as a graph of final pH versus initial pH, as shown in Figure 4.7. The PZC value of Fe$_3$O$_4$ NPs was found to be 6.50, indicating a neutral charge at pH 6.50. At pH values below 6.50, Fe$_3$O$_4$ NPs were positively-charged, while at pH values above 6.50, they were negatively-charged. However, after coating with PDDA, the PZC value of Fe$_3$O$_4$ NPs decreased to 6.25. This suggests that the PDDA coating provided a higher number of sites that can be protonated in an acidic medium, as explained by Celestino et al. (2018).
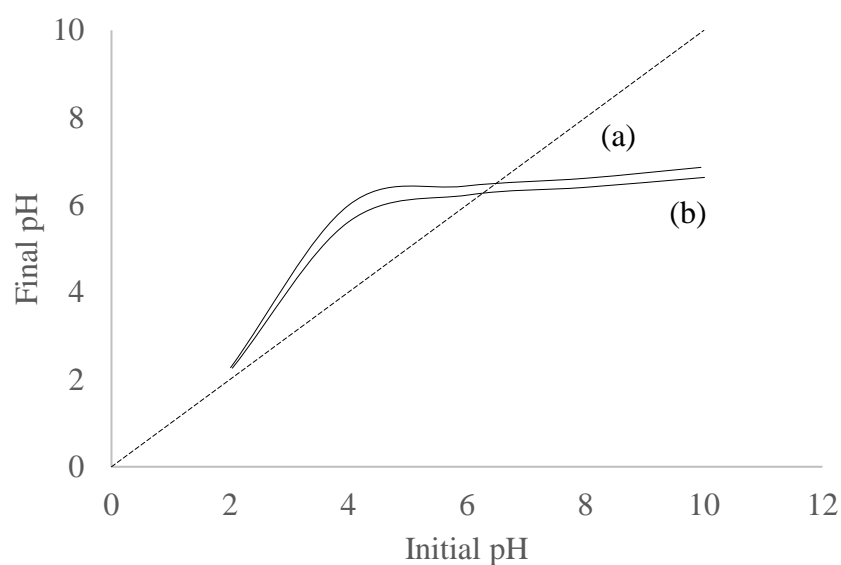
Figure 4.7: pH Drift Results of (a) Fe$_3$O$_4$ NPs and (b) PDDA/Fe$_3$O$_4$ NPs.

The graph of initial pH versus final pH can be interpreted as follows. For example, using PDDA/Fe$_3$O$_4$ NPs at pH 10.01, the initial pH of 10.01 resulted in a final pH of 6.63, indicating a positive charge that attracted and adsorbed OH$^-$ ions in the solution, leading to a decrease in pH. On the other hand, PDDA/Fe$_3$O$_4$ NPs with an initial pH of 4 that rose to pH 5.61 suggested that the NPs removed positively charged hydronium ions (H$_3$O$^+$) from the solution. The polymer coating effect was evident at an initial pH of 10.0 where Fe$_3$O$_4$ NPs could only reduce the solution pH to pH 6.86 while PDDA/Fe$_3$O$_4$ NPs could lower it further to pH 6.63. This implies that the PDDA coating introduced a more positive surface that could adsorb more Gram-negative *E. coli* in the water treatment process.
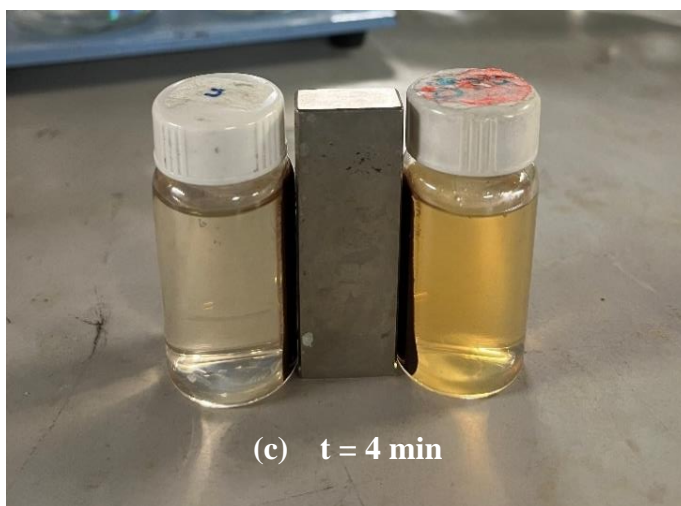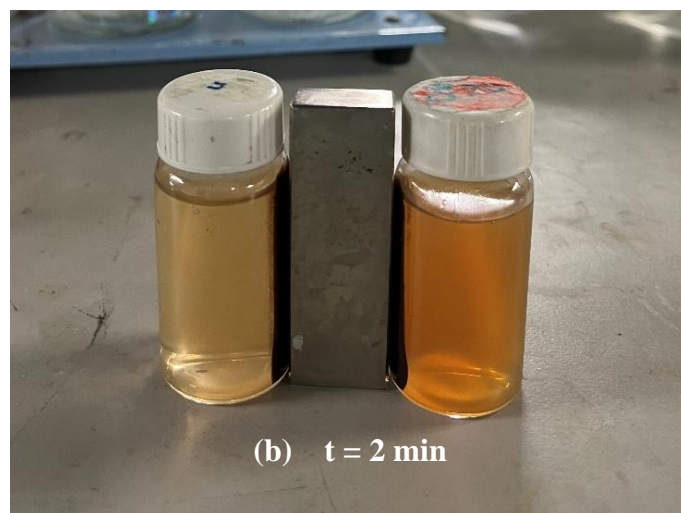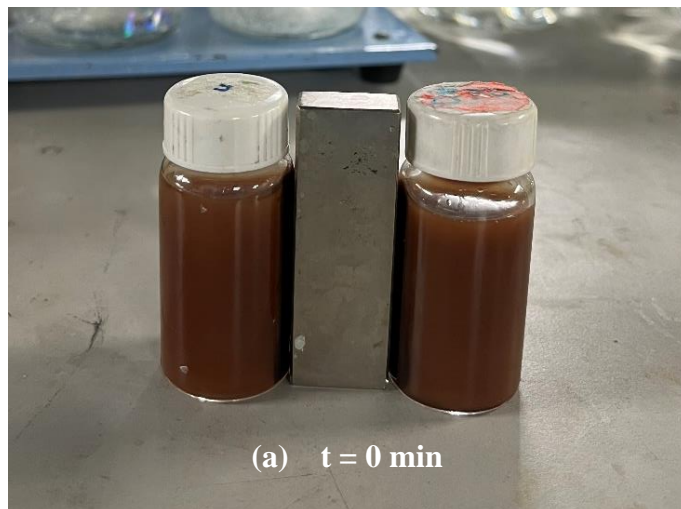
4.2   Magnetic Performance of PDDA/Fe$_3$O$_4$ NPs

In this study, 20 mL of distilled water was used to disperse 200 mg of PDDA/Fe$_3$O$_4$ and Fe$_3$O$_4$ NPs. To evaluate the magnetic responsive behavior of the samples, an external magnetic field was applied. The response of Fe$_3$O$_4$ and PDDA/Fe$_3$O$_4$ NPs to the external magnetic field over a 6-minute period is presented in Figure 4.8 (a) to (d).

From the results, it could be seen that a clearer solution was obtained for Fe$_3$O$_4$ NPs compared to PDDA/Fe$_3$O$_4$ NPs in the 6th minute which shown in Figure 4.8(d). This indicated that the PDDA/Fe$_3$O$_4$ NPs exhibited a slower response towards the magnetic field than the naked Fe$_3$O$_4$ NPs. This observation could be attributed to the functionalization of PDDA polymer which improved the stability and dispersion of the Fe$_3$O$_4$ NPs in water. The introduction of positively-charged PDDA polymer had increased the electrostatic repulsions between Fe$_3$O$_4$ NPs in water. In addition, the polymer coating might had reduced the size of NPs due to the reduced agglomeration between NPs (Khalkhali et al., 2015). However, SEM images in Chapter 4.1.1 did not showed a reduction in the size of Fe$_3$O$_4$ NPs, possibly because of their small size difference. Besides, the smaller size of NPs required a longer period of time to be collected by the magnetic field, as they were more affected by the Brownian motion (Khalkhali et al., 2015).

In short, both Fe$_3$O$_4$ and PDDA/Fe$_3$O$_4$ NPs possesed magnetic properties that allowed for magnetic separation to remove them from the

solution. Although PDDA coating decreased the magnetic performance of Fe_3O_4 NPs, separation of NPs through magnetic field could be still achieved, but it might require a longer period of time.
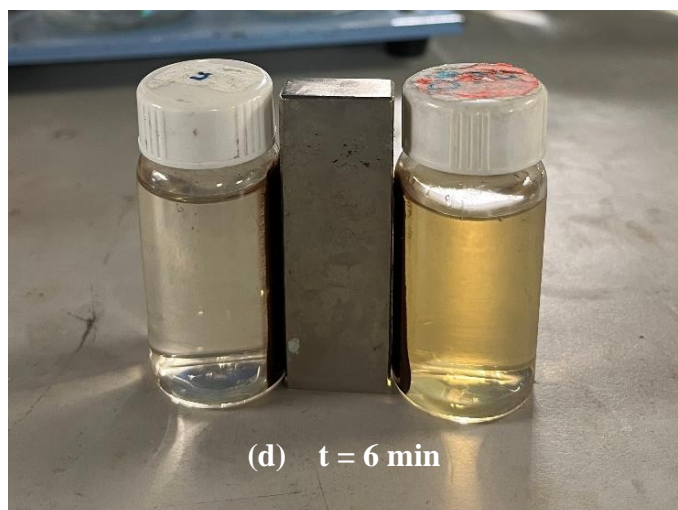

(a) t = 0 min

(b) t = 2 min

(c) t = 4 min

(d)   t = 6 min

Figure 4.8: Magnetic Performance of Fe_3O_4 NPs (left) and PDDA/Fe_3O_4 NPs (right) at Different Time Intervals.

4.3   Feasibility Study of PDDA/Fe_3O_4 NPs in the Degradation of *E. coli*

The effect of the dosage of PDDA/Fe_3O_4 NPs and the concentration of H_2O_2 in *E. coli* degradation process were studied in this experiment. All reacted solutions were subjected to the cultivation of *E. coli* in agar plate. Comparison of initial and final number of *E. coli* colonies in the agar plates was done to determine the efficiency of Fenton-like degradation process.

4.3.1   Effect of PDDA/Fe_3O_4 NPs Dosage

The effect of PDDA/Fe_3O_4 NPs dosage on the *E. coli* degradation was investigated. Two different PDDA/Fe_3O_4 NPs dosage used were 30 mg and 50 mg. The results are shown in Figure 4.9. Based on the result, both dosages (30 mg and 50 mg) for both samples (PDDA/Fe_3O_4 and Fe_3O_4 NPs) used could fully degrade the *E. coli* present in water sample.

Theoretically, an increase of PDDA/Fe_3O_4 NPs dosage would enhance the efficiency of *E. coli* degradation via Fenton-like reaction. This could be attributed to the increased availability of Fe^{2+} ions that were generated upon the reduction of Fe^{3+} ions by the Fe_3O_4 NPs. These Fe^{2+} ions catalysed the decomposition of H_2O_2 to form •OH, a strong oxidising agent that could degrade organic molecules including *E. coli.* In addition, a higher dosage of PDDA/Fe_3O_4 provided more active binding sites for *E. coli*, thereby increasing the likelihood of contact between *E. coli* and •OH. However, in this experiment,

no significant difference in the *E. coli* degradation efficiency was observed due to the excess supply of PDDA/Fe$_3$O$_4$ NPs. The use of 30 mg of both Fe$_3$O$_4$ and PDDA/Fe$_3$O$_4$ NPs was sufficient to fully degrade the *E. coli* present in the water sample.

Both samples were subjected to the same reaction condition with H$_2$O$_2$ present and the solution pH maintained at pH 7. No pH adjustment was done for the solutions, even though Fenton-like degradation favours pH 3 to 4. However, as heteregenous catalyst of PDDA/Fe$_3$O$_4$ and Fe$_3$O$_4$ NPs were used as the catalyst, Fenton-like reaction able to sucessfully degraded all of the *E. coli* present in the water sample.

In short, the study suggested that 30 mg of Fe$_3$O$_4$ and PDDA/Fe$_3$O$_4$ NPs were sufficient to degrade *E. coli* via Fenton-like reaction. Further study was needed to determine the lower limit of PDDA/Fe$_3$O$_4$ dosage for effective *E. coli* degration. Additionally, it is noteworthy that Fenton-like degradation could be conducted at normal water pH without any pH adjustment.
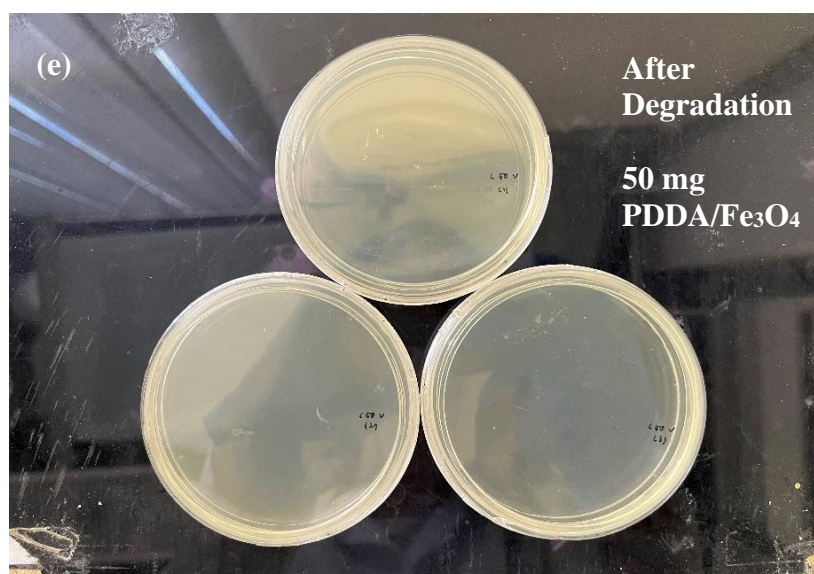
(b) After Degradation

30 mg Fe$_3$O$_4$

(c) After Degradation

30 mg PDDA/Fe$_3$O$_4$

(d) After Degradation

50 mg Fe$_3$O$_4$
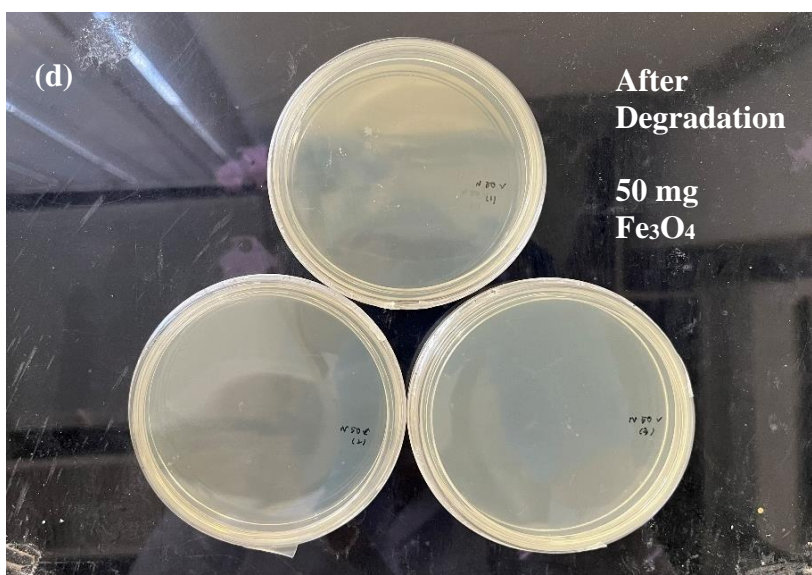
Figure 4.9: Agar Plate Results for Different Dosages of Fe_3O_4 and $PDDA/Fe_3O_4$ Used.

4.3.2   Effect of H_2O_2 Dosage

During the investigation of the effect of H_2O_2 dosage, one set of sample was conducted in the presence of H_2O_2 (4 mmol/L) whereas the other set of sample was conducted in the absence of H_2O_2. The results are shown in Figure 4.10. In the presence of H_2O_2, both Fe_3O_4 and $PDDA/Fe_3O_4$ NPs had fully degraded the available *E. coli* in the sample solution. In contrast, an average of two colonies were found on the agar plates of Fe_3O_4 NPs where no H_2O_2 was added, indicating the inefficiency of *E. coli* removal. However, without the addition of H_2O_2, the $PDDA/Fe_3O_4$ NPs still performed well in the removal of *E. coli*, leaving with no colonies observed on the agar plates.

H_2O_2 plays a crucial role as an oxidising agent in degrading *E. coli* via Fenton-like degradation process. In the absence of H_2O_2, Fenton-like degradation process was prohibited, *E. coli* could not be degraded. The coating of PDDA polymer had transformed the surface of Fe_3O_4 NPs into a more positively-charged surface. *E. coli* is a Gram-negative bacteria which possesses negative charge property. Hence, positively-charged $PDDA/Fe_3O_4$ NPs would attract and bind with the negatively-charged *E. coli* cell walls. Therefore, in the absence of H_2O_2, *E. coli* removal relied on adsorption process.

Based on the results in Figure 4.10 (c) and (d), the adsorption of *E. coli* was lower for Fe_3O_4 NPs compared to $PDDA/Fe_3O_4$ NPs. This might be due to

several reasons. Firstly, from Figure 4.7, Fe_3O_4 NPs had a less positively-charged surface than $PDDA/Fe_3O_4$ NPs. This resulted in a weaker electrostatic attraction between the Fe_3O_4 NPs and the *E. coli.* Hence, lesser *E. coli* would be attracted and adsorbed to the Fe_3O_4 NPs which indicated the poor removal scenario. Secondly, the smaller specific surface area of Fe_3O_4 than $PDDA/Fe_3O_4$ which shown in Table 4.2 had indicated that a lesser active site was available for the binding of *E. coli*. Therefore, the Fe_3O_4 NPs supplied were insufficient to uptake all of the *E. coli* present in the solution.

In short, 50 mg of $PDDA/Fe_3O_4$ NPs were sufficient for the removal of *E. coli* from the water sample even though H_2O_2 was absent. This had indicated the potential of $PDDA/Fe_3O_4$ in becoming a promising alternative for the *E. coli* removal.
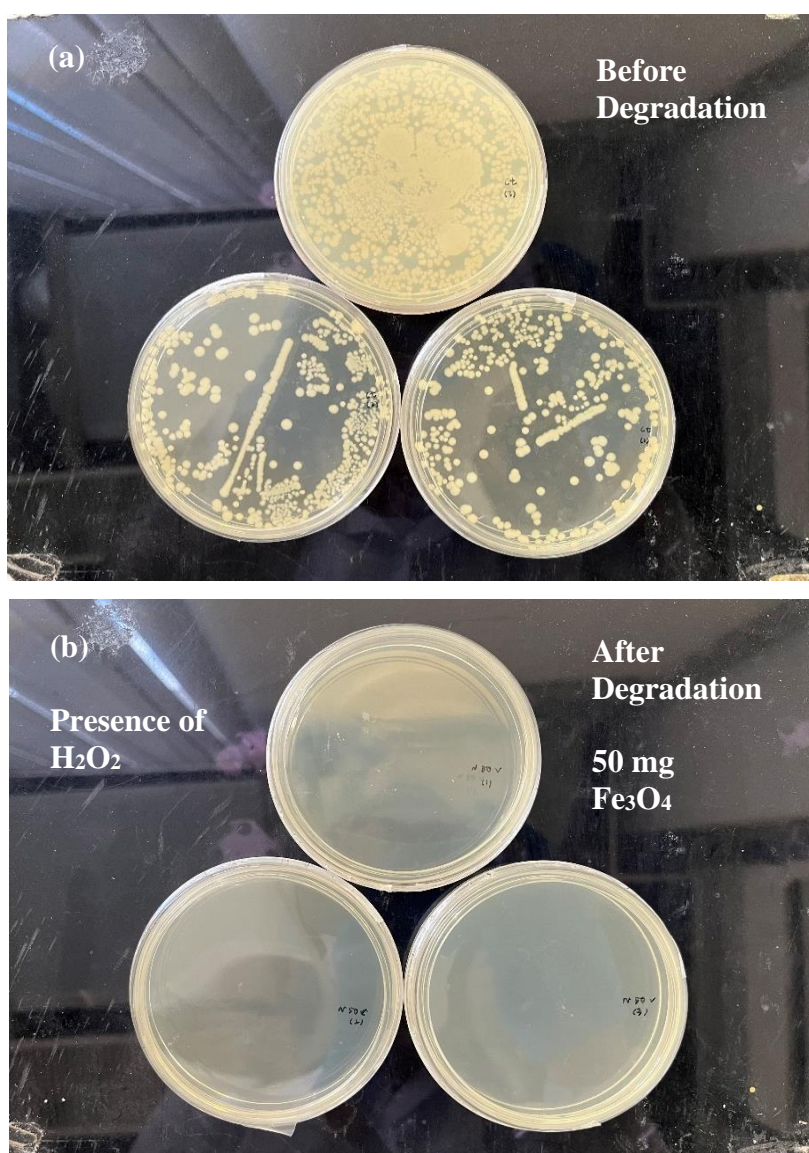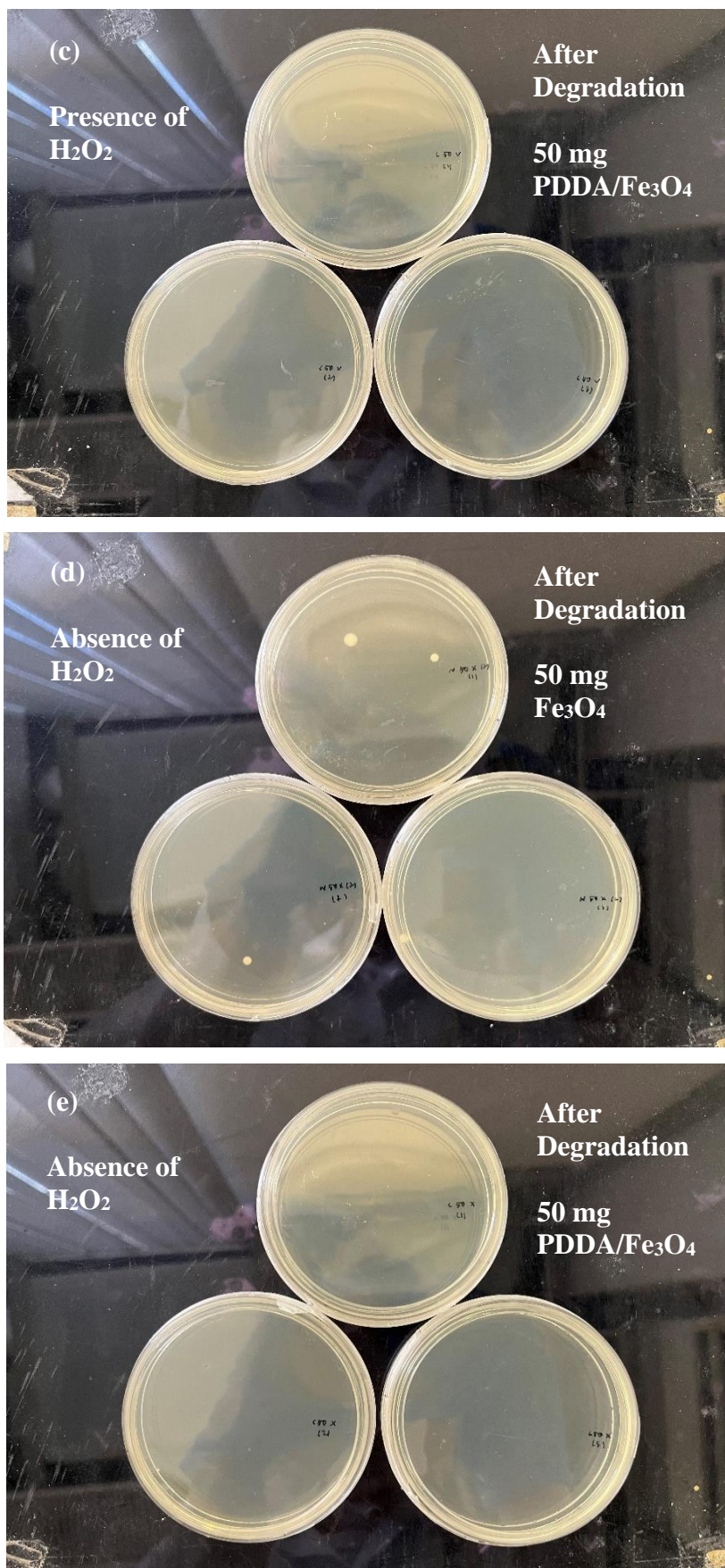
Figure 4.10: Agar Plate Results for the Absence and Presence of H_2O_2 in *E. coli*
Degradation.

4.3.3   SEM of Spent Fe₃O₄ NPs and PDDA/Fe₃O₄ NPs

SEM analysis was performed on both spent Fe_3O_4 and $PDDA/Fe_3O_4$ after the Fenton-like degradation process and the surface morphology was examined. Figure 4.11 (a) and (b) shows the SEM images of both Fe_3O_4 samples at a magnification of $\times 500$. Both samples were found to be having rough surfaces with obvious irregular pores on the surfaces. Conversely, the surface morphology of the fresh samples displayed smooth surfaces, as depicted in Figure 4.1 (a) and (b). The difference observed between fresh and spent Fe_3O_4 NPs was due to the corrosion of H_2O_2 happened in the Fenton-like degradation process. H_2O_2 is a strong oxidising agent which could attack the surface of Fe_3O_4 NPs, causing the irregular pores to be formed on the NPs surface. Notably, the corrosion was within acceptable limits as the Fe_3O_4 structure remained intact, albeit with altered surface features.
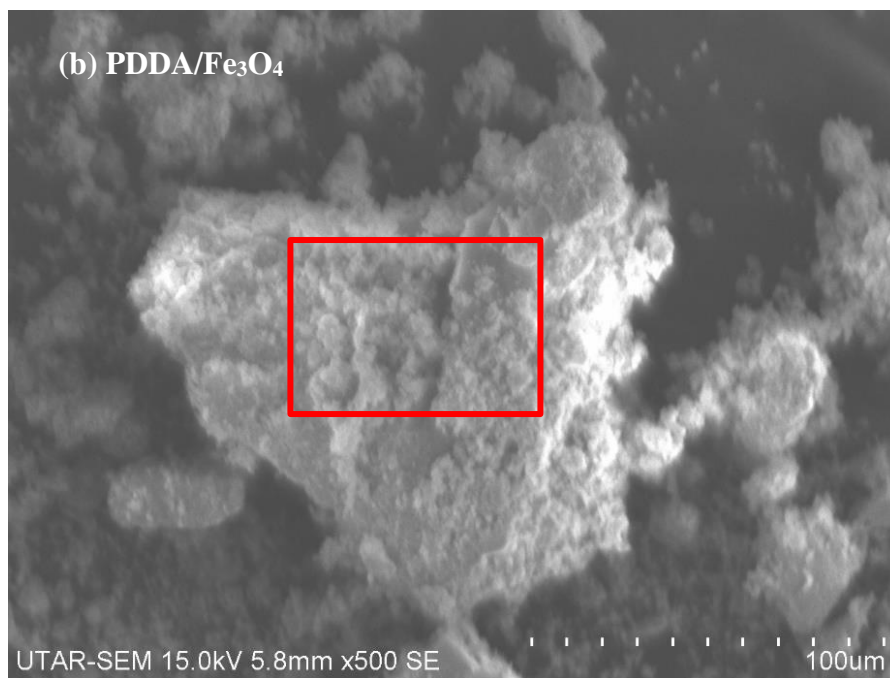

(a) Fe₃O₄

UTAR-SEM 15.0kV 5.8mm x500 SE   100um

Figure 4.11: SEM Images of Spent (a) Fe_3O_4 NPs and (b) $PDDA/Fe_3O_4$ NPs.

CHAPTER 5

CONCLUSION AND RECOMMENDATIONS

5.1   Conclusion

In this study, PDDA/Fe$_3$O$_4$ NPs were successfully prepared through one-pot synthesis method. The synthesized PDDA/Fe$_3$O$_4$ NPs were characterized by SEM/EDX, FTIR, BET, XRD, TGA and pH drift. SEM image showed the morphology of PDDA/Fe$_3$O$_4$ NPs were having smooth surfaces but in irregular shapes and uneven sizes. The SEM images also verified that the PDDA polymer coating process did not cause any damages on the surface of Fe$_3$O$_4$ NPs. Besides, agglomeration of NPs was less obvious in PDDA/Fe$_3$O$_4$ sample compared to Fe$_3$O$_4$ sample. EDX results indicated that Fe, O and Cl elements were found in Fe$_3$O$_4$ sample whereas Fe, O, C and N elements were found in PDDA/Fe$_3$O$_4$ sample. Moreover, FTIR analysis indicated the presence of several functional groups in PDDA/Fe$_3$O$_4$ NPs such as "Fe-O" bonds, "H-O-H" bending and "-OH" groups. On top of that, "C=C" and "C-N" groups at 1471 cm^{-1} and 1037 cm^{-1} respectively indicated the success of PDDA polymer coating on Fe$_3$O$_4$ NPs. For BET analysis, it showed that PDDA polymer coating had increased the specific surface area and decreased the pore diameter of Fe$_3$O$_4$ NPs. A larger adsorption area was provided in PDDA/Fe$_3$O$_4$ NPs. Next, XRD patterns verified that PDDA polymer coating process did not perturb the formation of crystal lattice of Fe3O4 NPs. In addition, TGA results showed a three-stage decomposition process of PDDA/Fe$_3$O$_4$ NPs, occurring at approximately 0 - 100 $^{\circ}$C, 100 – 250 $^{\circ}$C and 250 – 400 $^{\circ}$C. Lastly, pH drift results indicated the success of polymer coating process by showing that Fe$_3$O$_4$ NPs could only reduce the solution pH to pH 6.86 while PDDA/Fe$_3$O$_4$ NPs could lower it further to pH 6.63. Other than that, the magnetic performance of PDDA/Fe$_3$O$_4$ NPs was studied. A clearer solution was obtained for Fe$_3$O$_4$ NPs compared to PDDA/Fe$_3$O$_4$ NPs, indicating the slower magnetic response possessed by PDDA/Fe$_3$O$_4$ NPs.

The feasibility of PDDA/Fe$_3$O$_4$ NPs in the degradation of *E. coli* was studied. The focus process parameters were PDDA/Fe$_3$O$_4$ NPs dosage and H$_2$O$_2$ concentration. From the study, it could be concluded that both 30 mg and 50 mg PDDA/Fe$_3$O$_4$ NPs could fully degrade all *E. coli* present in the water sample. However, a 30 mg of PDDA/Fe$_3$O$_4$ NPs was sufficient for the complete degradation of *E. coli* via Fenton-like degradation. Apart from that, concentration of H$_2$O$_2$ had affected the degradation efficiency of *E. coli*. In the presence of H$_2$O$_2$, the degradation of *E. coli* was through Fenton-like process whereas in the absence of H$_2$O$_2$, *E. coli* could not be degraded instead it was adsorbed onto the surface of PDDA/Fe$_3$O$_4$ NPs.When H$_2$O$_2$ was present, 50 mg of both Fe$_3$O$_4$ and PDDA/Fe$_3$O$_4$ NPs could fully degrade *E. coli* in the soultion. However, in the absence of H$_2$O$_2$, 50 mg of Fe$_3$O$_4$ NPs was insufficient to fully adsorb *E. coli* present in the solution, leaving an average of two colonies being observed in the agar plates. In contrast, PDDA/Fe$_3$O$_4$ NPs were capable in *E. coli* removal without H$_2$O$_2$ being subjected. SEM was done on the spent PDDA/Fe$_3$O$_4$ NPs after the Fenton-like degradation process. SEM image showed the surface morphology of spent PDDA/Fe$_3$O$_4$ NPs was in rough surface with irregular pores on the surfaces. This was due to the corrosion of H$_2$O$_2$ but it was within the acceptable corrosion limits.

5.2 Recommendations for Future Work

In the study of the effect of PDDA/Fe$_3$O$_4$ NPs dosage, the lower limit for effective *E. coli* degradation should be studied. Apart from 30 mg and 50 mg, experiments on lower dosage of PDDA/Fe$_3$O$_4$ NPs like 5 mg and 10 mg should be performed. Besides, about the effect of H$_2$O$_2$ concentration on the Fenton-like degradation process, different concentration should be studied such as 1 mmol/L and 0.5 mmol/L to determine the lower and upper limit. Other than PDDA/Fe$_3$O$_4$ NPs dosage and H$_2$O$_2$ dosage, the pH and contact time should also be considered in the process parameters study. Different pH and contact time might resulted in different degradation efficiency. A shorter contact time with high degradation efficiency was preferable for industrial applications as the utilities cost would be decreased.

In addition to study the effect of process parameters, the reusability study should be performed to access the feasibility in practical applications. As seen in the SEM image, PDDA/Fe$_3$O$_4$ NPs which went through Fenton-like degradation process would be corroded by H$_2$O$_2$. Hence, studied should be carried out to determine the limit of PDDA/Fe$_3$O$_4$ NPs can be resued before it lose it ability in performing an effective *E. coli* degradation.

REFERENCES

Afroz, R. and Rahman, A., 2017. Health impact of river water pollution in Malaysia. *International Journal of ADVANCED AND APPLIED SCIENCES*, 4(5), pp.78-85.

Afroz, R., Masud, M., Akhtar, R. and Duasa, J., 2014. Water Pollution: Challenges and Future Direction for Water Resource Management Policies in Malaysia. *Environment and Urbanization Asia*, 5(1), pp.63-81.

Ali, A., Chiang, Y. and Santos, R., 2021. X-ray diffraction techniques for mineral characterization: A review for engineers of the fundamentals, applications, and research directions.

Ambroz, F., Macdonald, T., Martis, V. and Parkin, I., 2018. Evaluation of the BET Theory for the Characterization of Meso and Microporous MOFs. *Small Methods*, 2(11), p.1800173.

Araujo, F., Yokoyama, L., Teixeira, L. and Campos, J., 2011. Heterogeneous fenton process using the mineral hematite for the discolouration of a reactive dye solution. *Brazilian Journal of Chemical Engineering*, 28(4), pp.605-616.

Azmi, N., Ng, Q., Ahmad, A. and Low, S., 2012. Development of Magnetite Nano–composite Membrane for Membrane Defouling. *Journal of Applied Membrane Science & Technology*, 15(1).

Babuponnusami, A. and Muthukumar, K., 2014. A review on Fenton and improvements to the Fenton process for wastewater treatment. *Journal of Environmental Chemical Engineering*, 2(1), pp.557-572.

Bagal, M. and Gogate, P., 2014. Wastewater treatment using hybrid treatment schemes based on cavitation and Fenton chemistry: A review. *Ultrasonics Sonochemistry*, 21(1), pp.1-14.

Baresel, C., Schaller, V., Jonasson, C., Johansson, C., Bordes, R., Chauhan, V., Sugunan, A., Sommertune, J. and Welling, S., 2019. Functionalized magnetic particles for water treatment. *Heliyon*, 5(8), p.e02325.

Bertoldi, B., Richardson, S., Goodrich Schneider, R., Kurdmongkolthan, P. and Schneider, K., 2018. Preventing Foodborne Illness: E. coli "The Big Six". *EDIS*, 2018(1).

Bogachev, Y., Nikitina, A., Kostina, A., Sabitova, V., Pankov, V., Shutava, T., Petrova, E., Kotsikau, D., Natarov, V. and Livanovich, K., 2017. NMR Relaxation Efficiency of Aqueous Solutions of Composite Mg x Zn y Fe3−x−y O4 Nanoparticles. *Applied Magnetic Resonance*, 48(7), pp.715-722.

Bouasla, C., Samar, M. and Ismail, F., 2010. Degradation of methyl violet 6B dye by the Fenton process. *Desalination*, 254(1-3), pp.35-41.

Braz, V., Melchior, K. and Moreira, C., 2020. Escherichia coli as a Multifaceted Pathogenic and Versatile Bacterium. *Frontiers in Cellular and Infection Microbiology*, 10.

Bull, E., Madani, S., Sheth, R., Seifalian, A., Green, M. and Seifalian, A., 2014. Stem cell tracking using iron oxide nanoparticles. *International Journal of Nanomedicine*, p.1641-1653.

Burchacka, E., Pstrowska, K., Beran, E., Fałtynowicz, H., Chojnacka, K. and Kułażyński, M., 2021. Antibacterial Agents Adsorbed on Active Carbon: A New Approach for S. aureus and E. coli Pathogen Elimination. *Pathogens*, 10(8), p.1066.

Castro-Rios, K., Corpas, E., Cardenas, V. and Taborda, G., 2017. Inactivation efficiency of total coliforms and Escherichia coli in doped natural water by heterogeneous Fenton: Effect of process factors. *Journal of Materials and Environmental Sciences,* 8(1), pp. 364-369.

Celestino, G., Henriques, R., Shiguihara, A., Constantino, V., Melo, R. and Junior, J., 2018. Adsorption of gallic acid on nanoclay modified with poly(diallyldimethylammonium chloride). *Environmental Science and Pollution Research*, 26(28), pp.28444–28454.

Chai, L. G., 2020. The river water quality before and during the Movement Control Order (MCO) in Malaysia. *Case Studies in Chemical and Environmental Engineering*, 2, p.100027.

Chaturvedi, N. and Katoch, S., 2019. Effect of various parameters during degradation of toxic p-anisidine by Fenton's oxidation. *Applied Water Science*, 10(1).

Cheah, Y. K., Tay, L. W., Aida, A. A., Son, R., Nakaguchi, T. and Nishibuchi, M., 2015. Molecular characterization of Escherichia coli isolated from different food sources. *International Food Research Journal*, 22(1), pp.31-40.

Chen, J., Ju, Y. and Chen, H., 2019. One-pot synthesis of magnetic cationic adsorbent modified with PDDA for organic phosphonates removal. *Nano*, 14(02), p.1950019.

Chen, L., Zhou, Z., Shen, C. and Xu, Y., 2020. Inactivation of antibiotic-resistant bacteria and antibiotic resistance genes by electrochemical oxidation/electro-Fenton process. *Water Science and Technology*, 81(10), pp.2221-2231.

Chin, E., 2021. Report: E. coli bacteria found thriving in Johor's polluted Sungai Kim Kim. *malaymail*, [online] Available at: <https://www.malaymail.com/news/malaysia/2021/04/23/report-e.-coli-bacteria-found-thriving-in-johors-polluted-sungai-kim-kim/1968817> [Accessed 20 August 2022].

Chittoo, B. and Sutherland, C., 2019. Adsorption Using Lime-Iron Sludge–Encapsulated Calcium Alginate Beads for Phosphate Recovery with ANN- and RSM-Optimized Encapsulation. *Journal of Environmental Engineering*, 145(5).

Chye, F., Abdullah, A. and Ayob, M., 2004. Bacteriological quality and safety of raw milk in Malaysia. *Food Microbiology*, 21(5), pp.535-541.

Colombo, M., Carregal-Romero, S., Casula, M., Gutiérrez, L., Morales, M., Böhm, I., Heverhagen, J., Prosperi, D. and Parak, W., 2012. Biological applications of magnetic nanoparticles. *Chemical Society Reviews*, 41(11), p.4306-4344.

Costa, R., Lelis, M., Oliveira, L., Fabris, J., Ardisson, J., Rios, R., Silva, C. and Lago, R., 2006. Novel active heterogeneous Fenton system based on Fe3−xMxO4 (Fe, Co, Mn, Ni): The role of M2+ species on the reactivity towards H2O2 reactions. *Journal of Hazardous Materials*, 129(1-3), pp.171-178.

Croxen, M., Law, R., Scholz, R., Keeney, K., Wlodarska, M. and Finlay, B., 2013. Recent Advances in Understanding Enteric Pathogenic Escherichia coli. *Clinical Microbiology Reviews*, 26(4), pp.822-880.

Davodi, B., Jahangiri, M. and Ghorbani, M., 2018. Magnetic Fe_3O_4 @ polydopamine biopolymer: Synthesis, characterization and fabrication of promising nanocomposite. *Journal of Vinyl and Additive Technology*, 25(1), pp.41–47.

Deng, J., Jiang, J., Zhang, Y., Lin, X., Du, C. and Xiong, Y., 2008. FeVO4 as a highly active heterogeneous Fenton-like catalyst towards the degradation of Orange II. *Applied Catalysis B: Environmental*, 84(3-4), pp.468-473.

Domingues, E., Gomes, J., Quina, M., Quinta-Ferreira, R. and Martins, R., 2018. Detoxification of Olive Mill Wastewaters by Fenton's Process. *Catalysts*, 8(12), p.662.

Ellingham, S., Thompson, T. and Islam, M., 2017. Scanning Electron Microscopy-Energy-Dispersive X-ray (SEM/EDX): A Rapid Diagnostic Tool to Aid the Identification of Burnt Bone and Contested Cremains. *Journal of Forensic Sciences*, 63(2), pp.504-510.

Fajarwati, F., Ika Yandini, N., Anugrahwati, M. and Setyawati, A., 2020. Adsorption Study of Methylene Blue and Methyl Orange Using Green Shell (Perna Viridis). *EKSAKTA: Journal of Sciences and Data Analysis*, pp.92-97.

Feng, S., Wang, R., Bai, Y., Yang, S., Ma, Q., Yilihamu, A., Yang, S. and Luo, J., 2019. Fe3O4/SiO2/C nanocomposites for the fenton-like disinfection of Escherichia coli in water. *Materials Research Express*, 6(5), p.055032.

Garrido-Ramírez, E., Theng, B. and Mora, M., 2022. Clays and oxide minerals as catalysts and nanocatalysts in Fenton-like reactions — A review. *Applied Clay Science*, 47, pp.182-192.

Gehrke, I., Geiser, A. and Somborn-Schulz, A., 2015. Innovations in nanotechnology for water treatment. *Nanotechnology, Science and Applications*, p.1-17.

Ghaderpour, A., Ho, W., Chew, L., Bong, C., Chong, V., Thong, K. and Chai, L., 2015. Diverse and abundant multi-drug resistant E. coli in Matang mangrove estuaries, Malaysia. *Frontiers in Microbiology*, 6.

Girao, D., Girao, V., Irino, K. and Tardelli Gomes, T., 2006. Classifying Escherichia coli. *Emerging Infectious Diseases*, 12(8), pp.1297-1299.

Gosens, I., Post, J., de la Fonteyne, L., Jansen, E., Geus, J., Cassee, F. and de Jong, W., 2010. Impact of agglomeration state of nano- and submicron sized gold particles on pulmonary inflammation. *Particle and Fibre Toxicology*, 7(1), p.37.

Hajiali A. and Pirumyan G. P., 2018. Efficiency of Ozonation Disinfection in a Domestic Wastewater Treatment for Removing Existing Infectious Bacteria and Viruses and a Comparison with Chlorine Disinfection. *International Research Journal of Advanced Engineering and Science*, 3(2), pp.341-344.

Hassan, H. and Hameed, B.H., 2011. Decolorization of acid red 1 by heterogeneous Fenton-like reaction using Fe-ball clay catalyst. *International Conference on Environment Science and Engineering*, 8, pp. 232-236.

Huang, Y., Wang, Y. and Yan, X., 2010. Amine-Functionalized Magnetic Nanoparticles for Rapid Capture and Removal of Bacterial Pathogens. *Environmental Science & Technology*, 44(20), pp.7908-7913.

Isawi, H., 2020. Using Zeolite/Polyvinyl alcohol/sodium alginate nanocomposite beads for removal of some heavy metals from wastewater. *Arabian Journal of Chemistry*, 13(6), pp.5691-5716.

Jain, B., Singh, A., Kim, H., Lichtfouse, E. and Sharma, V., 2018. Treatment of organic pollutants by homogeneous and heterogeneous Fenton reaction processes. *Environmental Chemistry Letters*, 16(3), pp.947-967.

Jang, J., Hur, H., Sadowsky, M., Byappanahalli, M., Yan, T. and Ishii, S., 2017. EnvironmentalEscherichia coli: ecology and public health implications-a review. *Journal of Applied Microbiology*, 123(3), pp.570-581.

Jang, S., Kang, S., Kim, G., Rethinasabapathy, M., Haldorai, Y., Lee, I., Han, Y., Renshaw, J., Roh, C. and Huh, Y., 2018. Versatile Poly(Diallyl Dimethyl Ammonium Chloride)-Layered Nanocomposites for Removal of Cesium in Water Purification. *Materials*, 11(6), p.998.

Jiang, C., Gao, Z., Qu, H., Li, J., Wang, X., Li, P. and Liu, H., 2013. A new insight into Fenton and Fenton-like processes for water treatment: Part II. Influence of organic compounds on Fe(III)/Fe(II) interconversion and the course of reactions. *Journal of Hazardous Materials*, 250-251, pp.76-81.

Kaper, J., Nataro, J. and Mobley, H., 2004. Pathogenic Escherichia coli. *Nature Reviews Microbiology*, 2(2), pp.123-140.

Katouli M., 2010. Population structure of gut Escherichia coli and its role in development of extra-intestinal infections. *Iranian journal of microbiology*, 2(2), pp.59–72.

Khalkhali, M., Rostamizadeh, K., Sadighian, S., Khoeini, F., Naghibi, M. and Hamidi, M., 2015. The impact of polymer coatings on magnetite nanoparticles performance as MRI contrast agents: A comparative study. *DARU Journal of Pharmaceutical Sciences*, 23(1).

Khan, I., Saeed, K. and Khan, I., 2019. Nanoparticles: Properties, applications and toxicities. *Arabian Journal of Chemistry*, 12(7), pp.908-931.

Khan, S., Khan, S., Khan, L., Farooq, A., Akhtar, K. and Asiri, A., 2018. Fourier Transform Infrared Spectroscopy: Fundamentals and Application in Functional Groups and Nanomaterials Characterization. *Handbook of Materials Characterization*, pp.317-344.

Kodoth, V. and Jones, M., 2015. The Effects of Ultraviolet Light on *Escherichia coli. Journal of Emerging Investigators.*

Kwan, W. and Voelker, B., 2003. Rates of Hydroxyl Radical Generation and Organic Compound Oxidation in Mineral-Catalyzed Fenton-like Systems. *Environmental Science & Technology*, 37(6), pp.1150-1158.

Lakshmanan, R., 2013. *Application of Magnetic Nanoparticles and Reactive Filter Materials for Wastewater Treatment,* PhD thesis, Royal Institute of Technology, Stockholm.

Liu, D., 2014. Escherichia coli☆. *Reference Module in Biomedical Sciences.*
Lv, F., Lu, X., Song, J., Zhu, M., Wang, S., Xu, Y. and Chang, X., 2022. Enhanced Aramid/Al2O3 Interfacial Properties By PDDA-Modification for The Preparation of Composite Insulating Paper. *Research on Chemical Intermediates*, 48, pp.4815–4835.

Mahmood, T., Saddique, M., Naeem, A., Westerhoff, P., Mustafa, S. and Alum, A., 2011. Comparison of different methods for the point of Zero charge determination of NiO. *Industrial & Engineering Chemistry Research*, 50(17), pp.10017–10023.

McCrary, K., Harclerode Case, C., Gentry, T. and Aitkenhead-Peterson, J., 2013. Escherichia coli Regrowth in Disinfected Sewage Effluent: Effect of DOC and Nutrients on Regrowth in Laboratory Incubations and Urban Streams. *Water, Air and Soil Pollution*, 224(2).

Mevold, A., Hsu, W., Hardiansyah, A., Huang, L., Yang, M., Liu, T., Chan, T., Wang, K., Su, Y., Jeng, R., Wang, J. and Wang, Y., 2015. Fabrication of Gold Nanoparticles/Graphene-PDDA Nanohybrids for Bio-detection by SERS Nanotechnology. *Nanoscale Research Letters*, 10(1).

Mohd Razelan, F., Tahir, W. and Yahaya, N., 2018. Studies on the current state of water quality in the Segamat River. *IOP Conference Series: Earth and Environmental Science*, 140, p.012016.

Murthy S. K., 2007. Nanoparticles in modern medicine: State of the art and future challenges. *International Journal of Nanomedicine,* 2(2), pp. 129-141.

Nalbandian, L., Patrikiadou, E., Zaspalis, V., Patrikidou, A., Hatzidaki, E. and Papandreou, C., 2016. Magnetic Nanoparticles in Medical Diagnostic Applications: Synthesis, Characterization and Proteins Conjugation. *Current Nanoscience*, 12(4), pp.455–468.

Nidheesh, P., 2015. Heterogeneous Fenton catalysts for the abatement of organic pollutants from aqueous solution: a review. *RSC Advances*, 5(51), pp.40552-40577.

Nuengmatcha, P., Chanthai, S., Mahachai, R. and Oh, W., 2016. Sonocatalytic performance of ZnO/graphene/TiO2 nanocomposite for degradation of dye pollutants (methylene blue, texbrite BAC-L, texbrite BBU-L and texbrite NFW-L) under ultrasonic irradiation. *Dyes and Pigments,* 134, pp.487-497.

Odonkor, S. and Ampofo, J., 2013. Escherichia coli as an indicator of bacteriological quality of water: an overview. *Microbiology Research*, 4(1).

Odonkor, S. and Mahami, T., 2020. Escherichia coli as a Tool for Disease Risk Assessment of Drinking Water Sources. *International Journal of Microbiology*, 2020, pp.1-7.

Onkundi Nyangaresi, P., Zhang, B. and Shen, L., 2020. Effects of UV-LED Irradiation on E. coli in Water Disinfection. *E. Coli Infections - Importance of Early Diagnosis and Efficient Treatment*.

Ortiz Ortega, E., Hosseinian, H., Aguilar Meza, I., Rosales López, M., Rodríguez Vera, A. and Hosseini, S., 2022. *Material characterization techniques and applications*. Singapore: Springer.

Osuolale, O. and Okoh, A., 2015. Assessment of the Physicochemical Qualities and Prevalence of Escherichia coli and Vibrios in the Final Effluents of Two Wastewater Treatment Plants in South Africa: Ecological and Public Health Implications. *International Journal of Environmental Research and Public Health*, 12(10), pp.13399-13412.

Otaki, M., Yano, K. and Ohgaki, S., 1998. Virus removal in a membrane separation process. *Water Science and Technology*, 37(10), pp.107-116.

Owoseni, M., Olaniran, A. and Okoh, A., 2017. Chlorine Tolerance and Inactivation of Escherichia coli recovered from Wastewater Treatment Plants in the Eastern Cape, South Africa. *Applied Sciences*, 7(8), p.810.

Oyehan, T., Olabemiwo, F., Tawabini, B. and Saleh, T., 2020. The capacity of mesoporous fly ash grafted with ultrathin film of polydiallyldimethyl ammonium for enhanced removal of phenol from Aqueous Solutions. *Journal of Cleaner Production*, 263, p.121280.

Pal, S., Joardar, J. and Song, J., 2008. Removal of E. colifrom Water Using Surface-Modified Activated Carbon Filter Media and Its Performance over an Extended Use. *Environmental Science & Technology*, 42(10), pp.3906-3906.

Parekh, A., 2013. *Use of Magnetic Nanoparticles for Wastewater Treatment,* PhD thesis, Massachusetts Institute of Technology.

Pinto, M., Ramalho, P., Moreira, N., Gonçalves, A., Nunes, O., Pereira, M. and Soares, O., 2020. Application of magnetic nanoparticles for water purification. *Environmental Advances*, 2, p.100010.

Prabakaran M., Selvi S.T., Merinal, S. and Panneerselvam, A., 2012. Effect of ozonation on pathogenic bacteria. *Advances in Applied Science Research*, 3(1), pp.299-302.

Price, R. and Wildeboer, D., 2017. E. coli as an Indicator of Contamination and Health Risk in Environmental Waters. In: A. Samie, ed., *Escherichia coli - Recent Advances on Physiology, Pathogenesis and Biotechnological Applications*. London: Intech Open.

Qu, J., Dong, Y., Wang Y. and Xing, H., 2015. A novel sensor based on Fe3O4 nanoparticles–multiwalled carbon nanotubes composite film for determination of nitrite. *Sensing and Bio-Sensing Research*, 3, pp.74–78.

Rahmawati, R., Melati, A., Taufiq, A., Sunaryono, Diantoro, M., Yuliarto, B., Suyatman, S., Nugraha, N. and Kurniadi, D., 2017. Preparation of MWCNTFe3O4 Nanocomposites from Iron Sand Using Sonochemical Route. *IOP Conference Series: Materials Science and Engineering*, 202.

Rana, S. and Singh, R., 2016. Investigation of structural, optical, magnetic properties and antibacterial activity of Ni-doped zinc oxide nanoparticles. *Journal of Materials Science: Materials in Electronics*, 27(9), pp.9346-9355.

Rashed, M., Eltaher, M. and Abdou, A., 2017. Adsorption and photocatalysis for methyl orange and Cd removal from wastewater using TiO 2 /sewage sludge-based activated carbon nanocomposites. *Royal Society Open Science*, 4(12), p.170834.

Rivas, B., Espinosa, C. and Sánchez, J., 2018. Application of the liquid-phase polymer-based retention technique to the sorption of molybdenum(VI) and vanadium(V). *Polymer Bulletin*, 76(2), pp.539-552.

Rusevova, K., Kopinke, F. and Georgi, A., 2012. Nano-sized magnetic iron oxides as catalysts for heterogeneous Fenton-like reactions—Influence of Fe(II)/Fe(III) ratio on catalytic performance. *Journal of Hazardous Materials*, 241-242, pp.433-440.

Sahilah, A. M., Aishah, H., Noraida, I. and Azuhairi, A. A., 2010. Detection of Shiga Toxin 1 and 2 (stx1 and stx2) Genes in Escherichia coli O157:H7 Isolated from Retail Beef in Malaysia by Multiplex Polymerase Chain Reaction (PCR). *Sains Malaysiana*, 39(1), pp.57-63.

Samer, M., 2015. Biological and Chemical Wastewater Treatment Processes. *Wastewater Treatment Engineering*.

Samsudin, A. and Hacker, V., 2019. Preparation and Characterization of PVA/PDDA/Nano-Zirconia Composite Anion Exchange Membranes for Fuel Cells. *Polymers*, 11(9), p.1399.

Shah, M., Aziz, S., Zakaria, Z., Lin, L. and Goni, M., 2018. A Review on Pathogenic Escherichia coli in Malaysia. *Advances in Animal and Veterinary Sciences*, 6(2).

Siregar, J., Sebayang, K., Yuliarto, B. and Humaidi, S., 2020. XRD characterization of Fe3O4-ZnO nanocomposite material by the hydrothermal method. *AIP Conference Proceedings*, 2221, 110008.

Soon, A. and Hameed, B., 2011. Heterogeneous catalytic treatment of synthetic dyes in aqueous media using Fenton and photo-assisted Fenton process. *Desalination*, 269(1-3), pp.1-16.

Spit, T., van der Hoek, J., de Jong, C., van Halem, D., de Kreuk, M. and Perez, B., 2022. Removal of Antibiotic Resistance From Municipal Secondary Effluents by Ozone-Activated Carbon Filtration. *Frontiers in Environmental Science*, 10.

Stan, M., Lung, I., Soran, M., Opris, O., Leostean, C., Popa, A., Copaciu, F., Lazar, M., Kacso, I., Silipas, T. and Porav, A., 2019. Data on the Removal of Optilan Blue Dye from Aqueous Media Using Starch-Coated Green Synthesized Magnetite Nanoparticles. *Data in Brief 25*, 104165.

Thomas, N., Dionysiou, D. and Pillai, S., 2021. Heterogeneous Fenton catalysts: A review of recent advances. *Journal of Hazardous Materials*, 404, p.124082. Thommes, M., 2007. Textural Characterization of Zeolites and Ordered Mesoporous Materials by Physical Adsorption. *Studies in Surface Science and Catalysis*, p.495-XIII.

Tong, K., 2017. Preparation and biosorption evaluation of Bacillus subtilis/alginate–chitosan microcapsule. *Nanotechnology, Science and Applications*, Volume 10, pp.35-43.

Tong, M., Liu, F., Dong, Q., Ma, Z. and Liu, W., 2020. Magnetic Fe3O4-deposited flower-like MoS2 nanocomposites for the Fenton-like Escherichia coli disinfection and diclofenac degradation. *Journal of Hazardous Materials*, 385, p.121604.

Upadhyayula, V., Deng, S., Mitchell, M., Smith, G., Nair, V. and Ghoshroy, S., 2008. Adsorption kinetics of Escherichia coli and Staphylococcus aureus on single-walled carbon nanotube aggregates. *Water Science and Technology*, 58(1), pp.179-184.

Vergine, P., Salerno, C., Barca, E., Berardi, G. and Pollice, A., 2016. Identification of the faecal indicator Escherichia coli in wastewater through the β-D-glucuronidase activity: comparison between two enumeration methods, membrane filtration with TBX agar, and Colilert®-18. *Journal of Water and Health*, 15(2), pp.209-217.

Vermeulen, N., Keeler, W., Nandakumar, K. and Leung, K., 2007. The bactericidal effect of ultraviolet and visible light on Escherichia coli. *Biotechnology and Bioengineering*, 99(3), pp.550-556.

Walton, K. and Snurr, R., 2007. Applicability of the BET Method for Determining Surface Areas of Microporous Metal−Organic Frameworks. *Journal of the American Chemical Society*, 129(27), pp.8552-8556.

Wang, C., Liu, H. and Sun, Z., 2012. Heterogeneous Photo-Fenton Reaction Catalyzed by Nanosized Iron Oxides for Water Treatment. *International Journal of Photoenergy*, 2012, pp.1-10.

Wang, N., Zheng, T., Zhang, G. and Wang, P., 2016. A review on Fenton-like processes for organic wastewater treatment. *Journal of Environmental Chemical Engineering*, 4(1), pp.762-787.

Wang, S., 2008. A Comparative study of Fenton and Fenton-like reaction kinetics in decolourisation of wastewater. *Dyes and Pigments*, 76(3), pp.714-720.

Wang, W., Xiao, X., Chen, J. and Jia, L., 2015. Carboxyl modified magnetic nanoparticles coated open tubular column for capillary electrochromatographic separation of biomolecules. *Journal of Chromatography A*, 1411, pp.92-100.

Wani, S., Maker, J., Thompson, J., Barnes, J. and Singleton, I., 2015. Effect of Ozone Treatment on Inactivation of Escherichia coli and Listeria sp. on Spinach. *Agriculture*, 5(2), pp.155-169.

Xu L. and Wang J., 2011. A heterogeneous Fenton-like system with nanoparticulate zero-valent iron for removal of 4-chloro-3-methyl phenol. *Journal of Hazard Material*, 186, pp. 256–264.

Xu, L., Zhang, C., Xu, P. and Wang, X., 2018. Mechanisms of ultraviolet disinfection and chlorination of Escherichia coli: Culturability, membrane permeability, metabolism, and genetic damage. *Journal of Environmental Sciences*, 65, pp.356-366.

Yu, C., Lin, C., Liu, C., Cheng, T. and Tseng, W., 2010. Synthesis of poly(diallyldimethylammonium chloride)-coated Fe3O4 nanoparticles for colorimetric sensing of glucose and selective extraction of thiol. *Biosensors and Bioelectronics*, 26(2), pp.913-917.

Yusoff, A., Salimi, M. and Jamlos, M., 2017. Synthesis and characterization of biocompatible fe3o4 nanoparticles at different pH. *AIP Conference Proceedings.*

Zaliha, I. and Rusli, A., 2004. A study on hygienic standard of food premises and microbiological quality of food in Kota Bharu. Working Paper. Universiti Sains Malaysia.

Zhan, S., Yang, Y., Shen, Z., Shan, J., Li, Y., Yang, S. and Zhu, D., 2014. Efficient removal of pathogenic bacteria and viruses by multifunctional amine-modified magnetic nanoparticles. *Journal of Hazardous Materials*, 274, pp.115-123.

Zhang, X., Wang, W., Zhang, Y., Zeng, T., Jia, C. and Chang, L., 2018. Loading Cu-doped magnesium oxide onto surface of magnetic nanoparticles to prepare magnetic disinfectant with enhanced antibacterial activity. *Colloids and Surfaces B: Biointerfaces*, 161, pp.433-441.

Zhao, H., Zhang, G., Chong, S., Zhang, N. and Liu, Y., 2015. MnO2/CeO2 for catalytic ultrasonic decolorization of methyl orange: Process parameters and mechanisms. *Ultrasonics Sonochemistry*, 27, pp.474-479.

Zhong, D., He, F., Ma, W., Yuan, Y. and Wang, Z., 2018. Study on the Inactivation of Pseudomonas sp and the Degradation of Trichloroethylene by Fenton-Like Reaction. *Water*, 10(10), p.1376.

Zhou, T., Wang, M., He, X. and Qiao, J., 2019. Poly(vinyl alcohol)/poly(diallyldimethylammonium chloride) anion-exchange membrane modified with multiwalled carbon nanotubes for alkaline fuel cells. *Journal of Materiomics*, 5(2), pp.286–295.

Zimmer, J. and Slawson, R., 2002. Potential Repair of Escherichia coli DNA following Exposure to UV Radiation from Both Medium- and Low-Pressure UV Sources Used in Drinking Water Treatment. *Applied and Environmental Microbiology*, 68(7), pp.3293-3299.

APPENDICES

Appendix A: Preparation of 0.1 M NaCl Solution

0.1 M NaCl solution was needed as the solvent in the pH drift characterization test. However, the readily available NaCl in the laboratory is in solid form. To prepare a 0.1 M NaCl solution, calculation was done to determine the amount of solid NaCl needed to dissolve in 500 mL of distilled water.

$$Number\ of\ mol\ of\ NaCl = Molarity \times Volume \times Purity$$
$$= 0.1 \frac{mol}{L} \times 500\ mL \times \frac{1L}{1000ml} \times \frac{100}{99}$$
$$= 0.0505\ mol$$

$$Mass\ of\ NaCl = Number\ of\ mol\ of\ NaCl \times Molecular\ weight\ of\ NaCl$$
$$= 0.0505\ mol \times 58.44 \frac{g}{mol}$$
$$= 2.95\ g$$

Hence, to prepare a 0.1 M NaCl solution, a mass of 2.95 g of NaCl solid need to be added into 500 mL of distilled water.

Appendix B: Preparation of 0.8 % NaCl Solution

0.8 % NaCl solution was needed as the solvent in the serial dilution of *E. coli* solution. However, the readily available NaCl in the laboratory is in solid form. To prepare a 0.8 % NaCl solution, calculation was done to determine the amount of solid NaCl needed to dissolve in 500 mL of distilled water.

$$Concentration\ of\ NaCl = 0.8\ \%$$
$$= 0.0008\ \frac{g}{ml}$$

$$Mass\ of\ NaCl = Concentration\ of\ NaCl \times Volume\ of\ distilled\ water$$
$$= 0.0008\frac{g}{ml} \times 500\ ml$$
$$= 0.4\ g$$

Hence, to prepare a 0.8 % NaCl solution, a mass of 0.4 g of NaCl solid need to be added into 500 mL of distilled water.